Article

Structure

Infectivity of Dengue Virus Serotypes 1 and 2 Is Correlated with E-Protein Intrinsic Dynamics but Not to Envelope Conformations

Graphical Abstract

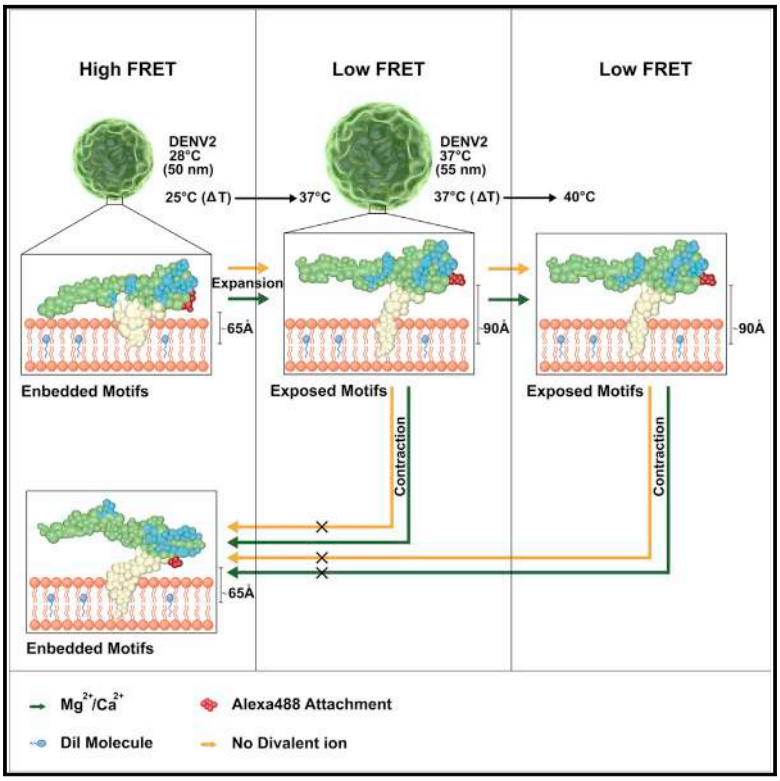

Highlights

- Mg^{2+}/Ca^{2+} mediate the temperature-dependent partial reversibility in DENV2 morphology
- MD show disruption of the inter-subunit salt bridges at the 5-fold vertex at $\geq 37°C$
- Loss of E-protein flexibility and intrinsic dynamics correlates to DENV2 infectivity
- DENV2 and DENV1 show divergent morphological and intrinsic dynamic behaviors

Authors

Kamal Kant Sharma, Xin-Xiang Lim, Sarala Neomi Tantirimudalige, ..., Peter J. Bond, Ganesh S. Anand, Thorsten Wohland

Correspondence

twohland@nus.edu.sg

In Brief

Sharma et al. have demonstrated that divalent ions alter the temperature-mediated DENV2 morphologies and the flexibility of the DENV2 E-protein domain III by disrupting the inter-subunit salt bridges at the 5-fold vertex. The dampening of the virus intrinsic dynamics, not the morphology, correlates to the reduced DENV2 infectivity.

Sharma et al., 2019, Structure *27*, 1–13
April 2, 2019
https://doi.org/10.1016/j.str.2018.12.006

CellPress

Please cite this article in press as: Sharma et al., Infectivity of Dengue Virus Serotypes 1 and 2 Is Correlated with E-Protein Intrinsic Dynamics but Not to Envelope Conformations, Structure (2018), https://doi.org/10.1016/j.str.2018.12.006

Infectivity of Dengue Virus Serotypes 1 and 2 Is Correlated with E-Protein Intrinsic Dynamics but Not to Envelope Conformations

Kamal Kant Sharma,[1] Xin-Xiang Lim,[1] Sarala Neomi Tantirimudalige,[1] Anjali Gupta,[1] Jan K. Marzinek,[1,5] Daniel Holdbrook,[1,5] Xin Ying Elisa Lim,[2] Peter J. Bond,[1,5] Ganesh S. Anand,[1] and Thorsten Wohland[1,3,4,6,*]
[1]Department of Biological Sciences, National University of Singapore, Centre of Bioimaging Sciences, 14 Science Drive 4, Singapore 117543, Singapore
[2]Duke-National University of Singapore Graduate Medical School, 8 College Road, Singapore 169857, Singapore
[3]Department of Chemistry, National University of Singapore, 14 Science Drive 4, Singapore 117543, Singapore
[4]Centre for Bioimaging Sciences, National University of Singapore, 14 Science Drive 4, Singapore 117557, Singapore
[5]Bioinformatics Institute (A*STAR), 30 Biopolis Street, #07-01 Matrix, Singapore 138671, Singapore
[6]Lead Contact
*Correspondence: twohland@nus.edu.sg
https://doi.org/10.1016/j.str.2018.12.006

SUMMARY

Dengue is a mosquito-borne virus with dire health and economic impacts. Dengue is responsible for an estimated 390 million infections per year, with dengue 2 (DENV2) being the most virulent strain among the four serotypes. Interestingly, it is also in strains of this serotype that temperature-dependent large-scale morphological changes, termed "breathing," have been observed. Although the structure of these morphologies has been solved to 3.5-Å resolution, the dynamics of the viral envelope are unknown. Here, we combine fluorescence and mass spectrometry with molecular dynamics simulations to provide insights into DENV2 (NGC strain) structural dynamics in comparison with DENV1 (PVP 159). We observe hitherto unseen conformational changes and structural dynamics of the DENV2 envelope that are influenced by both temperature and divalent cations. Our results show that for DENV2 and DENV1 the intrinsic dynamics, but not the specific morphologies, are correlated with viral infectivity.

INTRODUCTION

Dengue virus (DENV) is responsible for a wide range of clinical manifestations ranging from acute febrile illness to life-threatening dengue hemorrhagic fever and dengue shock syndrome (Gubler, 2002, 2012; Kyle and Harris, 2008; Morens and Fauci, 2008) with an estimated 390 million infections annually (Bhatt et al., 2013). DENV has four characterized serotypes (DENV1–4), and infection by one serotype does not confer immunity against heterologous serotypes (Guzman et al., 2010). Instead, it may cause a more severe and life-threatening form of dengue infection through antibody-dependent enhancement (Halstead, 2012a; b, 2013). Despite such a disease burden, there are no alternative therapeutics (Bennett et al., 2010; Halstead, 2012b; Holmes, 2003; Sabchareon et al., 2012) with the exception of a few low-efficacy (~30% overall) vaccines (Halstead, 2012b; Sabchareon et al., 2012) on the market.

Evidence suggests that flaviviruses explore an ensemble of morphologies at equilibrium, referred to as viral structural dynamics or "breathing" (Dowd et al., 2014; Dowd and Pierson, 2011; Lok et al., 2008; Rey, 2013), and is an essential aspect of the life cycle of many viruses (Dowd et al., 2014; Witz and Brown, 2001). These distinct morphologies arise due to large- and small-scale conformational changes in the organization of surface glycoproteins, which results from the virus experiencing perturbations in temperature, pH, or host-protein interactions (Mukhopadhyay et al., 2005). DENV1–4 display various surface glycoprotein (E protein) organizations at temperatures above 34°C, as experienced in the human body (37°C), compared with lower temperatures, such as those found in mosquitoes (28°C) (Fibriansah et al., 2013, 2015; Kostyuchenko et al., 2014; Lim et al., 2017b; Zhang et al., 2013). Temperature-dependent transitions in E-protein organization are most prominent in specific strains of DENV2, which acquires a "bumpy" form at temperatures above 35°C in contrast to the "smooth" form at 28°C (Lok et al., 2008). It has been suggested that such large-amplitude reversible morphological changes in the DENV2 envelope might be the basis of "breathing," which could be blocked by the insertion of an antibody (Lok et al., 2008). However, the formation of the DENV2 bumpy form has been observed to be irreversible, at least for two different strains, DENV2 16681 and DENV2 New Guinea strain (NGC) (Fibriansah et al., 2013; Zhang et al., 2013). Furthermore, plaque assays performed by incubating DENV2 at either 28°C or at 37°C indicated that the smooth and bumpy morphologies are not correlated with infectivity (Fibriansah et al., 2013). This raises at least two questions regarding DENV conformations, dynamics and infectivity. First, are the morphological changes really irreversible? Structural experiments have been conducted in buffers that lack divalent ions contrary to the plaque assays, which are conducted in cell-culture media in the presence of Ca^{2+} and Mg^{2+}. As the structure and function of several viruses depends on divalent

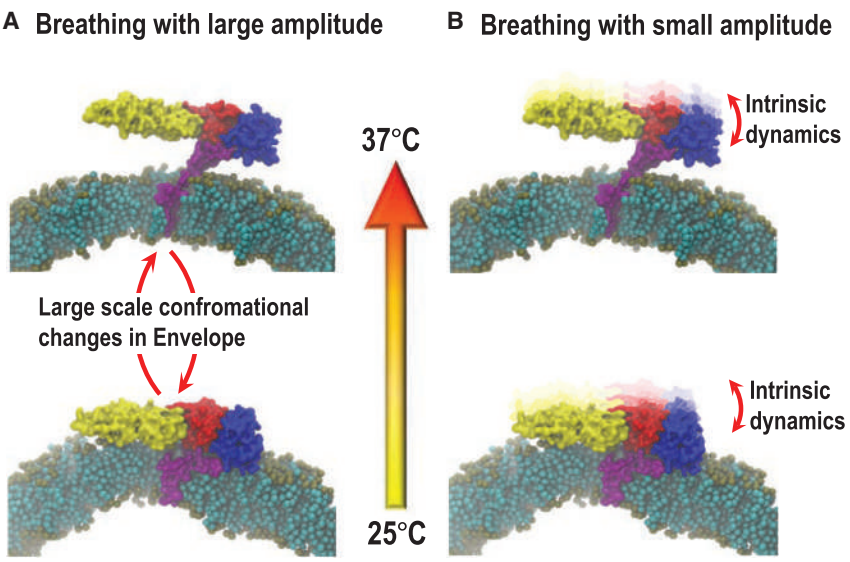

Figure 1. Schematic Representation of DENV2 "Breathing" with (A) Large and (B) Small Amplitude

(A and B) DENV2 E protein, constituting the viral envelope, has four domains, E-DI (yellow-colored residues), E-DII (red-colored residues), E-DIII (blue-colored residues), and the stem domain (purple-colored residues), which connect to a transmembrane region. (A) DENV2 undergoes temperature dependent large-scale conformational changes in the organization of surface E proteins between 25°C and 37°C. In smooth DENV2, the E protein lies close to the virus bilayer. In bumpy DENV2, the E proteins undergo an outward motion and a 15-Å gap between lipid bilayer and E-protein layer is formed that in turn results in the expansion of the virus from 50-nm diameter (at 28°C) to a diameter of 55 nm (at 37°C) (Fibriansah et al., 2013, 2015). However, unlike as depicted in the scheme, lowering of the temperature does not induce reversal of large-scale conformational changes in the E protein, thus defying the concept of DENV2 "breathing." (B) DENV2 breathing also encompasses the E-protein structural dynamics that take place in both the smooth and bumpy form at smaller time and length scales (Zhang et al., 2013), termed intrinsic dynamics.

ions (Cotmore et al., 2010; Kruse et al., 1982; Sherman et al., 2006; Shirley et al., 1981), is it possible that DENV conformations also depend on divalent ions? Second, is it possible that there exist viral protein dynamics over faster time and smaller length scales, as suggested by Zhang et al. (2013) that are related to infectivity? For the sake of clarity, in this article we distinguish between changes in overall DENV morphology, which are induced by temperature changes and are accessible by electron microscopic structural investigations (to date called "breathing"), and DENV intrinsic dynamics, which describe fast protein dynamics at smaller amplitudes and are not related to any persistent structures (Figure 1).

We have previously followed the large-scale outward conformational motion of envelope proteins (expansion) in DENV2 and DENV1 between 25°C and 40°C by time-resolved Förster resonance energy transfer (trFRET), using dual-labeled virus particles that carried Alexa 488-TFP as FRET donor on the E protein and DiI (tetramethylindocarbocyanine perchlorate) as FRET acceptor within the lipid bilayer (Lim et al., 2017b) (Figure 2A). In trFRET, the energy transfer from donor to acceptor, which is strongly distance dependent, influences the donor fluorescence lifetime. The Förster radius, R_0, of the pair is 59 Å, which is on the order of the distance between E protein and bilayer (Fibriansah et al., 2013). Changes in the large-scale morphology of DENV alter the distances between the E protein and the viral lipid membrane (Haas et al., 1978) and in turn influence the donor fluorescence lifetime. However, we had not investigated the temperature-dependent reversibility (contraction) of those morphological changes in dependence on divalent ions, nor did we investigate fast low-amplitude dynamics.

Here, we confirm that the formation of the DENV2 bumpy form is irreversible in the absence of divalent cations. For this, we used DENV2 (NGC) and DENV1 (PVP 159) (DENV2 and DENV1 in the rest of the article refer specifically to NGC and PVP 159 strains, respectively), produced and purified from C6/36 *Aedes albopictus* mosquito cells at 28°C. We further investigated whether these temperature-dependent large-scale morphological changes are reversible in the presence of divalent cations. In addition to large-scale morphological changes, we also followed intrinsic dynamics of the single DENV envelope protein by FRET fluctuation spectroscopy (FRET-FCS), in both the presence and absence of divalent cations. We support the fluorescence results with amide hydrogen/deuterium exchange mass spectrometry (HDXMS), molecular dynamics (MD) simulations, and infectivity measurements via plaque-forming assays. Taken together our results show that, at least for DENV2 and DENV1, viral intrinsic dynamics, but not the specific morphologies, correlate with DENV infectivity.

RESULTS AND DISCUSSION

FRET-Pair-Labeled DENV1 and DENV2 Show Temperature-Dependent Lifetimes

DENV2 E protein, constituting the viral envelope, has four domains (E-DI [residues 1–52; 132–193; 280–296], E-DII [residues 53–131; 194–279], E-DIII [residues 297–394], and the stem domain [residues 395–486]) that connect to a transmembrane region (Modis et al., 2003; Rey et al., 1995). The pseudo-atomic-resolution map of the virus shell (Kuhn et al., 2002) showed that the E protein forms 90 dimers on the smooth surface of the mature virus (Fibriansah et al., 2013). Cryoelectron microscopy (cryo-EM) (Fibriansah et al., 2013; Zhang et al., 2013) and HDXMS (Lim et al., 2017b) studies revealed that these E-protein dimers undergo an outward motion during a temperature change from 28°C to 37°C, leading to a morphological expansion from a "smooth" to a "bumpy" form of the virus. In buffer containing 150 mM sodium ion solution, this temperature-dependent morphological change was irreversible even when the temperature was subsequently lowered to 28°C. By investigating the outward motion of E proteins from the

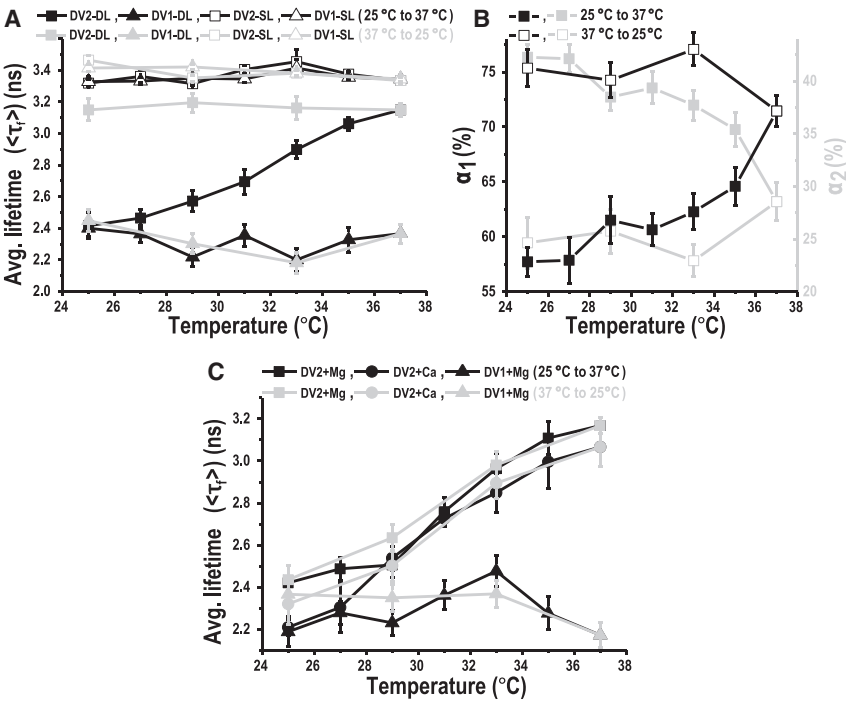

Figure 2. Structural Transitions of DENV2 and DENV1 Between 25°C and 37°C in Absence and Presence of Mg^{2+}/Ca^{2+} Ions

The lifetime traces for single- and dual-labeled viruses were fitted to a mono- and biexponential decay model, respectively. (A) Average fluorescence lifetimes ($<\tau_f>$) of AF488-TFP for donor-only-labeled, $<\tau_{f,\ SL}>$ (open triangles/squares) and dual-labeled, $<\tau_{f,\ DL}>$ (filled triangles/squares) for 5×10^7 PFU/mL DENV2 (squares) and 5×10^7 PFU/mL DENV1 (triangles). The data were collected during temperature increase from 25°C to 37°C (black triangles/squares) followed by decrease from 37°C to 25°C (gray triangles/squares). (B) Lifetime amplitudes corresponding to populations with low-FRET (black open/filled squares) and high-FRET (gray open/filled squares). The data were collected during temperature increase from 25°C to 37°C (filled squares) followed by decrease from 37°C to 25°C (open squares). By fitting dual-labeled viruses to a biexponential decay model, two lifetimes were calculated. The value of ~3.7 ns corresponds to unquenched or expanded DENV2, whereas the second lifetime of ~1.2 ns represents DENV2 particles that were unexpanded or undergo contraction. (C) Average fluorescence lifetimes ($<\tau_f>$) for DENV2 in the presence of 1 mM Mg^{2+} (squares) or 2 mM Ca^{2+} (circles) and for DENV1 in the presence of 1 mM Mg^{2+} (triangles). The data were collected during temperature increase from 25°C to 37°C (black circles/triangles/squares) followed by decrease from 37°C to 25°C (gray circles/triangles/squares). Error bars represent standard deviations (SDs) of six different experimental replicates in both DENV2 and DENV1 viruses, and the values are provided in Table S1.

virus bilayer for DENV2 and DENV1 using trFRET (Lim et al., 2017b), we confirmed the temperature-dependent morphological changes, due to virus expansion, seen by EM and HDXMS. However, the regions in the E protein that are responsible for the donor lifetime changes in trFRET were not identified.

Since Alexa 488-TFP attacks primary amines, the labeling site on the E protein will depend on the accessibility of lysines and their N-terminal amine moiety. To identify the labeled regions, we tagged the viruses with N-hydroxysulfosuccinimide ester of biotin, which labels free amino groups, similar to the fluorescence tag Alexa 488-TFP. The biotinylated peptides were captured using high-affinity biotin-streptavidin interactions. The position of biotinylated residues was determined by peptide mapping using liquid chromatography-tandem mass spectrometry. The majority of biotins were found coupled to the lysine residue (K344) in the region spanning peptides 335_I–345_V (Figure S1A) of the DENV2 E-DIII. K344 in the motif 335_I–345_V is proximal (<10 Å) to the DENV2 E-protein peptide residues 307_V–338_K (denoted by orange color in Figure S1A) that undergo outward conformational changes between 28°C and 37°C (Lim et al., 2017b). This suggests that trFRET monitors the temperature-dependent large-scale conformational changes related to E-DIII of DENV2.

Similarly, for DENV1, the majority of biotins were found coupled to the lysine residue (K110 and K135) in the region spanning peptides 95_T–110_K and 129_I–136_Y (denoted by red color in Figure S1B) of DENV1 E-DII. The motifs 95_T–110_K and 129_I–136_Y are in proximity to the DENV1 E-protein peptide residues 238_T–260_H (DENV1 E-DII) and 152_N–173_Q (DENV1 E-DI), respectively (denoted by orange color in Figure S1B) that undergo conformational changes between 37°C and 40°C (Lim et al., 2017b).

As control measurements, we measured donor-only-labeled virus at 25°C, which could be fitted with a single lifetime of 3.47 ± 0.07 ns for both DENV1 and DENV2 (Figure 2A). The donor- and acceptor-labeled viruses exhibited two lifetimes at the same temperature, indicating at least two distinguishable virus morphologies. The decay of DENV2 had an average lifetime of 2.42 ± 0.05 ns (Figure 2B) and was best fitted with two discrete (long and short) lifetime components of 3.72 ± 0.1 ns ($<\tau_1>$) and 1.18 ± 0.1 ns ($<\tau_2>$) (Figure S2B) having populations of 57% ± 2% (α_1) and 43% ± 2% (α_2) (Figure 2A), respectively. Note that we cannot exclude the existence of morphologies with very short lifetimes or with lifetimes close to the two principal components. Both would not be resolvable within these measurements. However, as we will show below, it is the population of these lifetimes rather than the lifetimes themselves that report on morphological changes. The donor fluorescence intensity decays of DENV1 had an average lifetime of 2.37 ± 0.1 ns (Figure 2B) and were also best fitted with two discrete lifetimes with values similar to those of DENV2 (3.7 ± 0.1 ns [$<\tau_1>$] and 1.14 ± 0.1 ns [$<\tau_2>$]), with α_1 and α_2 measured as 46% ± 2% and 54% ± 2%, respectively (Figure S2E), indicating viral structural heterogeneity. The fact that the lifetimes for dual-labeled viruses are significantly shorter than the average lifetimes for corresponding single-labeled viruses indicates the existence of FRET at a population averaged distance of ~65 Å (Figure S1C) between virus-lipid bilayer and its E-protein scaffold. Interestingly, these discrete lifetimes ($<\tau_1>$ and $<\tau_2>$) remained constant over the full temperature range from 25°C and 40°C, and only the population

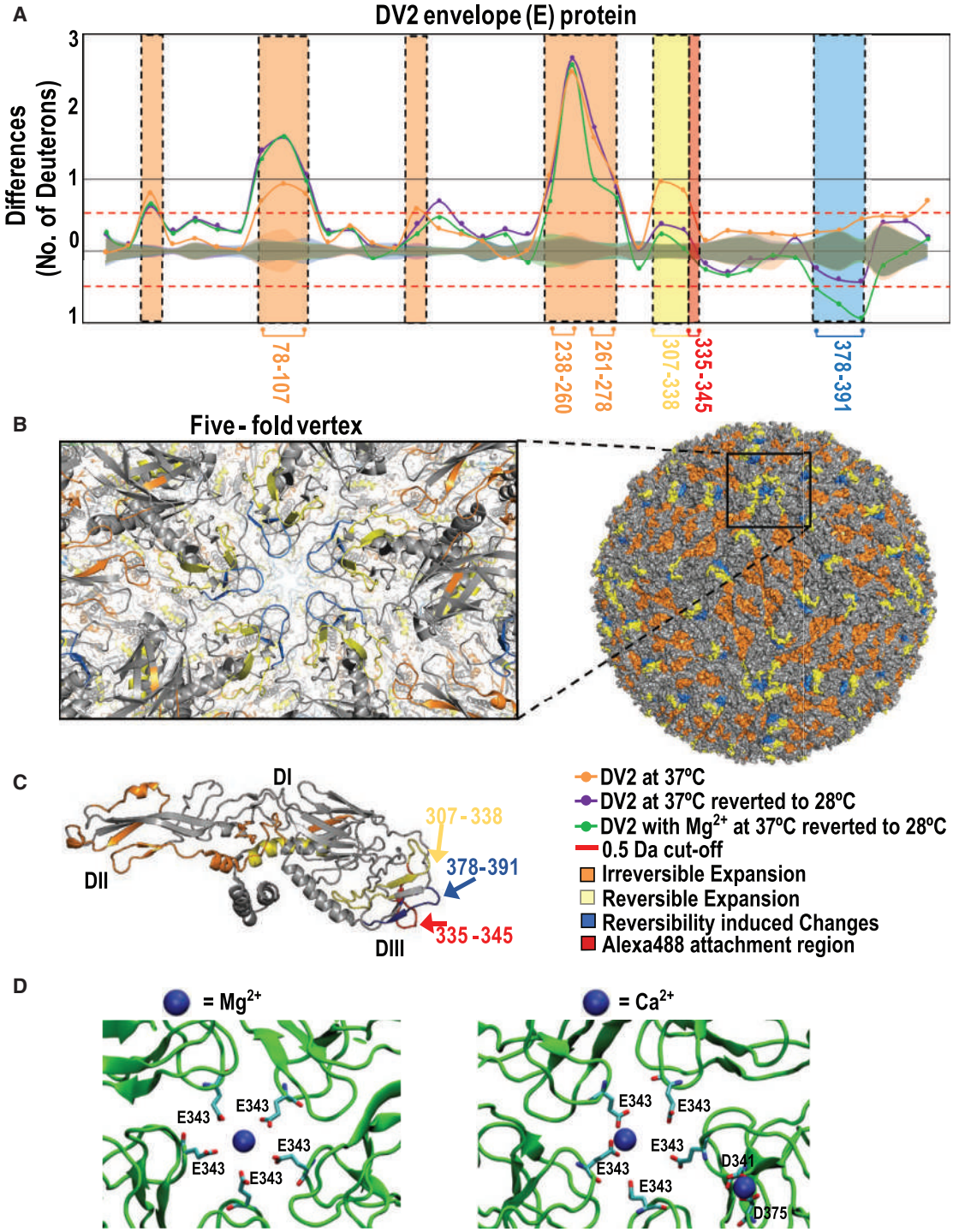

Figure 3. Non-uniform Temperature-Specific Changes in DENV2 in Absence and Presence of 1 mM Mg^{2+} at 37°C and 28°C by HDXMS, and Equilibrated Coordination of the Active Mg^{2+} or Ca^{2+} Binding Sites Based on MD Simulations

(A–C) HDXMS Difference plot (A) for temperature-induced differences (t = 1 min) in E protein from DENV2 at 37°C (orange line) and after reversal of temperature to 28°C in absence (violet line) and presence (green line) of 1 mM Mg^{2+}. The difference plot displays the differences in exchange between the two temperatures indicated in peptides protein-wide (y axis) with each dot representing a pepsin fragment peptide, listed from the N terminus to C terminus. y axis, differences in deuterons; x axis, pepsin fragment peptides. Differences in deuterium exchange above 0.5 D are considered significant (red dashed lines). Standard error for each peptide is shown as overlapping shaded regions along the x axis and colored according to the conditions in the difference plots. Orthogonal views of the differences in deuterium exchange in (B) viral particle surface and (inset) 5-fold vertex, and (C) E-protein peptides with temperature changes mapped onto the respective cryo-EM structures (PDB: 3J27). Regions with yellow color represent regions (V_{307}–K_{338} and G_{426}–A_{445}) with reversible expansion, orange color

(legend continued on next page)

(α_1 and α_2) of molecules corresponding to these lifetimes showed changes. This indicated a population interchange between the expanded ($<\tau_1>$) and unexpanded ($<\tau_2>$) virus morphologies with respect to temperature. As a consequence of this population interchange and the fact that our data contain only two populations, an increase in the value of α_1 will lead to a decrease in the value of α_2 by the same amount. Thus, henceforth in this article we will report the population corresponding to only the long lifetime (α_1) and the average lifetime. Data for individual lifetimes are provided in Supplemental Information.

DENV2, but not DENV1, Shows Mg^{2+}-/Ca^{2}-Dependent Morphological Changes between 25°C and 37°C

In the past, DENV morphological expansion had only been investigated in aqueous solutions containing monovalent ions alone (Fibriansah et al., 2013; Lim et al., 2017b; Zhang et al., 2013, 2015). However, the MD that led to this expansion were not addressed, raising several questions. Are all viral particles expanding equally? Are the morphological changes reversible, i.e., are the viral particles in thermal equilibrium?

First, as control, we confirmed the morphological expansions of both DENV1 and DENV2 during the transition from 25°C to 37°C. We then investigated reversibility of the morphological changes when the temperature was lowered back to 25°C, to mimic the transition between human- and mosquito-specific environments.

An increase in temperature from 25°C to 37°C in steps of 2°C led to an increase of the average fluorescence lifetime, $<\tau_f>$ (2.42 ± 0.05 ns → 3.18 ± 0.05 ns) and the long-lifetime population, α_1 (57% ± 2% → 72% ± 3%) for DENV2 (Figures 2A and 2B). The increase in $<\tau_f>$ indicated that the average distance between the labeled E-DIII and viral membrane bilayer increased from ~65 Å to ~90 Å (Figure S1C), while the difference in the values of α_1 at 37°C and 25°C indicated only ~15% from the total labeled DENV2 viruses underwent morphological transitions. This heterogeneity in DENV2 structures is consistent with the literature, where only ~22% of DENV2 particles show homogeneity in virus morphology (Zhang et al., 2013). A similar structural heterogeneity is reported for other flaviviruses (Dowd et al., 2014). With stepwise decrease in temperature from 37°C to 25°C, a marginal or no change in the values of $<\tau_f>$ and α_1 indicates no changes in the average distance between the labeled E-DIII and the viral membrane (Figures 2B and S1C). This result is in line with the literature (Fibriansah et al., 2013; Lim et al., 2017b; Zhang et al., 2013, 2015) and confirms the irreversibility of temperature-dependent DENV2 morphological changes in absence of divalent cations.

The introduction of divalent cations (Mg^{2+} and Ca^{2+}) does not significantly alter the population that undergoes structural transitions (Figures S2C and S2D). In addition to this, the similar values obtained for $<\tau_f>$ either at 25°C or 37°C (Figure 2C), suggest that divalent cations do not interfere with the viral heterogeneity. However, with stepwise reversal in temperature from 37°C to 25°C, a decrease in values of the $<\tau_f>$ (~3.2 ns → ~2.3 ns) (Figure 2C) and α_1 (~72% → ~58%) (Figures S2C and S2D) were observed for DENV2. This reversal in $<\tau_f>$ values (~2.4 ns → ~3.2 ns → ~2.3 ns) suggests that DENV2 expansion becomes at least partially reversible in the presence of divalent cations.

We used HDXMS to identify the exact DENV2 E-protein regions that underwent reversible conformational changes due to the temperature reversal from 37°C to 28°C. HDXMS has mapped DENV2 E-protein motifs that undergo conformational changes during expansion from 28°C to 37°C (Lim et al., 2017b) including E-DIII (307_V–338_K), E-DII (78_G–107_F and 238_T–278_F), E-DI (21_V–30_C), the second and third stem helices (431_I–448_S), and transmembrane helices (465_I–486_L) (Lim et al., 2017b). Surprisingly, only one of the six aforementioned E-protein motifs, namely the E-DIII region spanning peptides 307_V–338_K, showed temperature-dependent reversal (Figure 3A). In line with the literature (Butrapet et al., 2011; Fibriansah et al., 2013; Lim et al., 2017b; Lok et al., 2008; Messer et al., 2014), this result also confirmed that DENV2 E protein does not behave as a rigid body.

Furthermore, unlike peptide 307_V–338_K, the E-DIII region spanning peptides 378_I–391_F showed Mg^{2+}-dependent negative deuterium exchange when reverting to 28°C (Figure 3A). The results showed that only two E-DIII motifs undergo temperature-dependent reversible large-scale conformational changes and thus indicate a minimal change in the DENV2 bumpy morphology when reverting to 28°C (Figure S3). This is in contrast to picornavirus-like "breathing" whereby viruses undergo temperature-dependent large-scale reversible conformational changes (Jimenez et al., 2000; Katpally et al., 2009; Li et al., 1994; Pulli et al., 1998; Witz and Brown, 2001).

Thus, in addition to establishing E-DIII flexibility during both outward and inward conformational changes, these results also prove that DENV2 undergoes only partial "breathing" and only in the presence of divalent cations. However, such partial DENV2 morphological changes are physiologically relevant as E-DIII is involved in host-receptor binding (Crill and Roehrig, 2001; Hung et al., 2004; Modis et al., 2003; Rey et al., 1995). It is also possible that such divalent cation-dependent large-scale E-DIII flexibility is essential for optimal virus infectivity.

Interestingly, peptide 378_I–391_F constitutes the apex region of the junction where E-protein units are arranged into 5-fold vertices (represented by blue color in Figure 3B and inset), indicating that the divalent cation-dependent E-DIII conformational changes can be localized to the DENV2 5-fold vertices. Taken together, our data identify the DENV2 E-protein region loci that undergo Mg^{2+}- and Ca^{2+}-dependent reversible large-scale conformational changes. Furthermore, DENV1 showed in absence (Figures 2B and S2E) and presence (Figures 2C and S2F) of divalent cations only small conformational changes, consistent with evidence from the literature that DENV1 does not show large-scale conformational changes in this temperature range (Lim et al., 2017b; Zhang et al., 2013).

represents regions (G_{78}–F_{107} and T_{238}–F_{278}) with irreversible expansion, and blue color represents regions (I_{378}–F_{391}) with reversibility-induced changes, when virus temperature was lowered to 28°C. Red color indicates the Alexa 488-TFP-attachment site (I_{335}–V_{345}) on E protein.

(D) MD simulation snapshots of the E protein at the pentamer interface showing the number of atomic contacts within 3.0 nm between Mg^{2+}/Ca^{2+} cations and the I_{335}–V_{345} peptide.

Divalent Cation Binding Disrupts the Inter-subunit Salt Bridges at the 5-Fold Vertex of DENV2

We investigated the interaction between Mg^{2+}/Ca^{2+} ions and the surface E proteins at the 5-fold symmetry vertices of the "bumpy" DENV2 virus, using explicitly solvated, atomic-resolution MD simulations. MD simulations (Dror et al., 2010; Perilla et al., 2015; Zhao et al., 2013) and coarse-grained methodologies enable access to virus dynamics (Bond et al., 2007; Marrink et al., 2007; Reddy et al., 2015). Overall, MD simulations suggested that Mg^{2+} ions interacted with the Glu343 (E343) while Ca^{2+} ions interacted either with Glu343 or two Asp residues, 341 (D341) and 375 (D375) (Figure 3D). Interestingly, E343 and D341 lie within the Alexa 488-TFP attachment region spanning peptide 335_I–345_V (Figure 3C) of the DENV2 E-DIII. Additionally, residue 375 is in close proximity to the region showing Mg^{2+}-dependent reversible large-scale conformational changes (Figure 3C). Again, E343 and D341/D375 lie within peptides that constitute the apex region of the junction where E-protein units are arranged into 5-fold vertices (represented by blue color in Figure 3B and inset), supporting the notion that divalent ions bind at DENV2 5-fold vertices.

Furthermore, the initial simulation snapshots of the pentameric interface showed spontaneous formation of multiple inter-subunit salt bridges between E343 and K344 from adjacent subunits, i.e., between chains I and II, II and III, IV and V, and V and I (Figure 4A). These salt bridges presumably stabilize/lock the protein-protein interfaces in the "bumpy" state of the virion. The electrostatic potential and visualization of the resultant field lines of the E-protein pentamer (Figures 4B and 4C) revealed the presence of an electrostatic "funnel" expected to drive divalent cations toward the 5-fold vertex of the symmetry, thus increasing the local divalent cation concentration. Indeed, after 200 ns of simulation, Ca^{2+} ions were found to have stably associated with the E343 side-chain carboxylate oxygen of three (chains I, IV, and V) out of five chains (Figure 4A). Comparisons between the initial and the final snapshots of pairs of E-protein interfaces and the corresponding time-series plots for chains I and II (Figure 4D) showed that the salt bridge remained stable over the course of the simulation where Ca^{2+} ion did not bind to E343. On the other hand, a concomitant breakage of the E343-K344 salt bridge was observed in the case of chains IV–V (Figure 4E) and V–I (Figure 4F) due to binding of Ca^{2+} to E343 at ~20 ns and ~120 ns, respectively.

Based on these observations, we hypothesize that divalent cations have the ability to "soak" the protein 5-fold interface, breaking the inter-chain salt bridges by binding to acidic residues and, thereby, reducing the stability of the "bumpy" state. While beyond the scope of the present study, it would be of interest to support this notion via mutational studies.

DENV2 E-DIII Loses Temperature and Divalent Cation-Dependent Flexibility at 40°C

During dengue fever, DENV is further exposed to temperatures as high as 40°C. Thus, we investigated the temperature-dependent E-DIII large-scale conformational changes when DENV2 and DENV1 transit to 40°C before reverting to 25°C.

An increase in temperature from 37°C to 40°C resulted in no or marginal increase in the values of $\langle\tau_f\rangle$ (Figure 5A) and α_1 (Figure S5A) for DENV2, indicating no further DENV2 E-protein conformational changes, as reported previously (Lim et al., 2017b). With the stepwise reversal in temperature from 40°C to 25°C in steps of 4°C, marginal or no change in the values of $\langle\tau_f\rangle$ (Figure 5) and α_1 (Figure S5) were observed both in the absence and the presence of divalent cations. This absence of DENV2 E-protein large-scale conformational changes contrasts with the effects observed between 25°C and 37°C in the presence of Mg^{2+} and Ca^{2+} ions, indicating an irreversible bumpy morphology of DENV2 at 40°C. Thus, in absence of any further large-scale conformational changes, as compared with that of 37°C (Lim et al., 2017b), the formation of an irreversible bumpy morphology of DENV2 at 40°C probably indicates the incomplete binding of divalent cations, which hindered their ability to "soak" the E protein at the 5-fold interface. Interestingly, a recent study with Zika virus supported the fact that a hydrogen-bonding interaction network within the ZIKV envelope protein contributes to the virus structural stability as well as *in vivo* pathogenesis (Gallichotte et al., 2017). To check this hypothesis, we compared the interaction between Ca^{2+} ions and the surface E proteins at the 5-fold symmetry vertices of the "bumpy" DENV2 virus at 37°C with that of the other two temperatures (either at 28°C or at 40°C), using MD simulations (Figure S4). We observed that the increase in temperature resulted in a higher number of interactions between divalent ions and the peptide 335_I–345_V (Figure S4B), due to the raised kinetic energy in the system leading to higher dynamics of divalent ions and, hence, collision rate with the peptide. At the end of the simulation time, it was also observed that divalent ions bind to the E343 residue at all three (28°C, 37°C, and 40°C) temperature conditions (Figure S4C), thus breaking the salt bridges in all cases. Thus, no significant differences in binding of divalent ions at the 5-fold interface were observed during simulations. One reason for this may be that the weak restraints applied to the protein backbone, necessary to maintain the 5-fold symmetry of the isolated pentamer, likely mask any temperature-dependent large-scale conformational changes. Another possible hypothesis for the different effects of divalent ions on the reversibility of DENV2 DIII at 37°C and 40°C could be the stability of E-protein dimers on the virus surface. A recent study has shown that the dimer-dissociation constant for DENV2 E protein is very temperature sensitive and ranges from <1 μM at 25°C to 50 μM at 41°C, due to a large exothermic enthalpy of binding of −79 kcal/mol (Kudlacek et al., 2018). Thus, this temperature-sensitive 50-fold reduction in dimerization ability of E proteins may lead to the formation of an irreversible bumpy DENV2 morphology when heated to 40°C.

Furthermore, in both the absence (Figures 5A and S5C) and presence (Figures 5B and S5D) of divalent cations, an increase in temperature from 37°C to 40°C resulted in increased values of $\langle\tau_f\rangle$ (2.4 ± 0.05 ns → 3.2 ± 0.05 ns) (Figure 2B) and α_1 (43% ± 3% → 65% ± 4%) (Figure 2A) for DENV1. Again, the difference in the values of α_1 at 37°C and 40°C indicated that, similar to DENV2, only ~22% of DENV1 underwent large-scale morphological changes. In contrast to DENV2, these DENV1 E-protein large-scale conformational changes were reversible when reverting to temperatures below 37°C. The results showed that DENV1 exhibits reversible large-scale morphological changes in the temperature range from 25°C to 40°C. The result confirms that the high sequence and structural homology of DENV1 and DENV2 E proteins do not translate into their

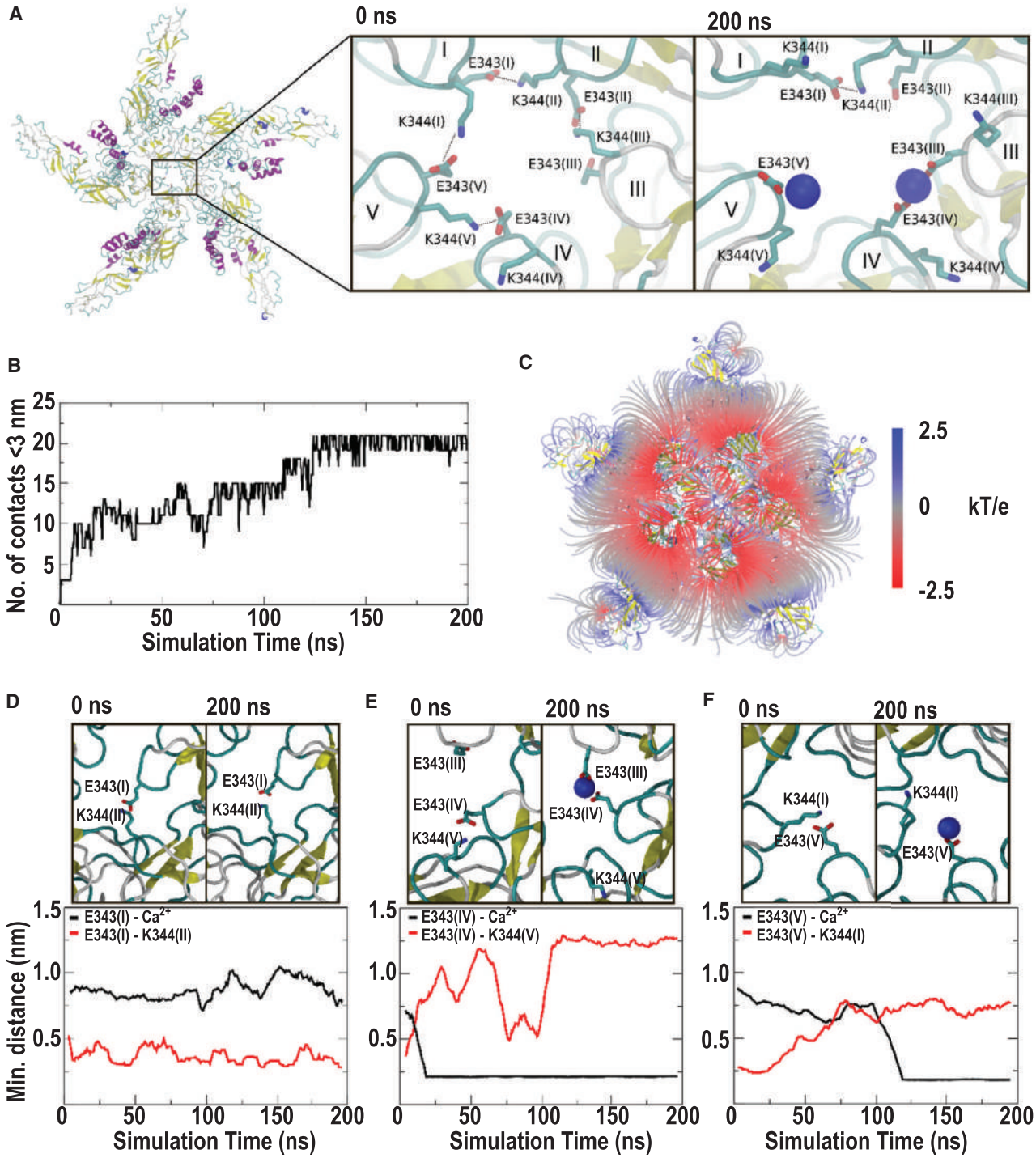

Figure 4. MD Simulations Reveal an Electrostatic Funnel for Calcium Binding and Salt Bridge Disruption at the E-Protein 5-Fold Vertex

(A) Initial and final snapshots of the pentamer (bottom view).

(B) Number of atomic contacts within 3.0 nm between Ca^{2+} cations and the 335_I–345_V peptide.

(C) Lines indicate the direction of the electrostatic field for the E-protein pentamer (top view), colored by potential energy value from −2.5 kT/e (red) to 2.5 kT/e (blue).

(D–F) Initial and final snapshots of the interface between chains I and II (D), IV and V (E), and V and I (F). Below each snapshot, corresponding time-dependent minimum distances are shown for E343–Ca^{2+} and E343–K344. In all protein snapshots, the secondary structure is shown in cartoon representation, with residue side chains in CPK wireframe format, and Ca^{2+} cations shown as blue spheres.

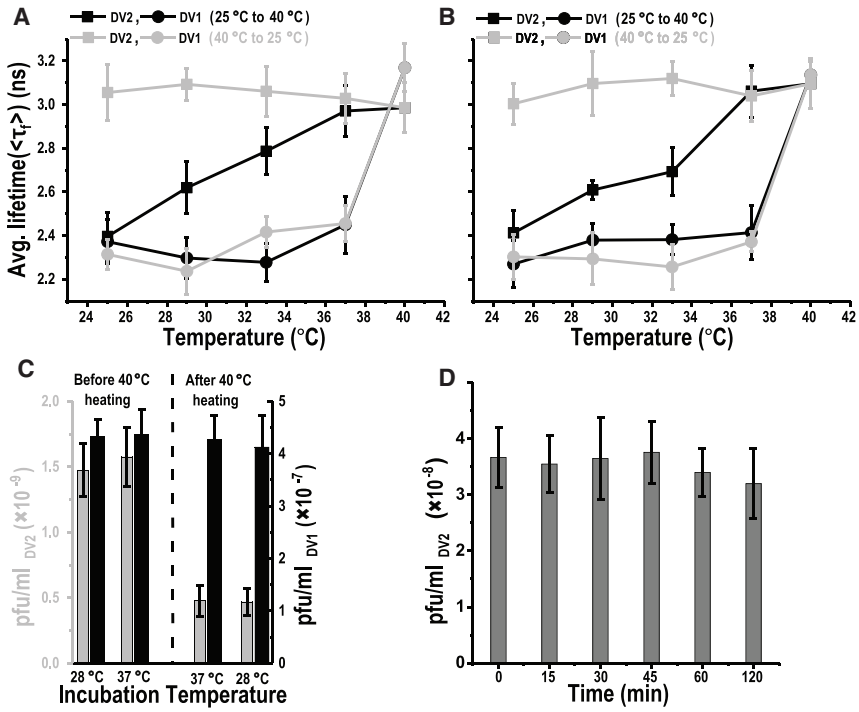

Figure 5. Structural Transitions and Infectivity of DENV2 and DENV1 Between 25°C and 40°C in Absence and Presence of Mg^{2+} Ions

(A) Average fluorescence lifetimes ($<\tau_f>$) for dual-labeled 5 × 10^7 PFU/mL DENV2 (squares) and 5 × 10^7 PFU/mL DENV1 (circles). The data were collected during temperature increase from 25°C to 40°C (black circles/squares) followed by decrease from 40°C to 25°C (gray circles/squares). (B) Average fluorescence lifetimes ($<\tau_f>$) for dual-labeled DENV2 (squares) and DENV1 (circles) in the presence of 1 mM Mg^{2+}. The data were collected during temperature increase from 25°C to 40°C (black circles/squares) followed by decrease from 40°C to 25°C (gray circles/squares). Error bars represent SDs of six different experimental replicates in both DENV2 and DENV1 viruses, and the values are provided in Table S2.

(C) Histogram showing plaque-forming virus titers performed at 1 hr incubation of either DENV2 (gray bars) or DENV1 (black bars) with BHK21 cells at temperatures of either 28°C or 37°C. Plaque assay was performed with both viruses before and after experiencing 40°C to have attained either flexible or locked E-protein conformation. Error bars represent SDs of three different experimental duplicates in both DENV2 and DENV1 viruses.

(D) Histogram showing infectivity-time-course plaque-forming DENV2 titers performed with BHK21 cells at 37°C. Viruses were incubated in buffer at 37°C for different durations (0, 15, 30, 45, 60, and 120 min) followed by their addition to BHK21 cells, and plaque assay was performed as explained in STAR Methods. DENV2 infectivity was measured at these time points to investigate any change in plaque-forming units due to time-dependent DENV2 aggregation. Error bars represent SDs of two different experimental duplicates in DENV2 viruses. No significant effect of DENV2 aggregation on its infectivity was observed, at least under our experimental conditions.

homologous morphologies (Fibriansah et al., 2013; Lim et al., 2017b; Zhang et al., 2013). In addition, these changes are independent of the presence of divalent cations and thus may indicate a higher structural stability of DENV1, due to stronger intra-dimeric E-protein contacts, as compared with DENV2 (Kostyuchenko et al., 2014).

DENV2 Loses Virus Infectivity due to Loss of Divalent Cation-Dependent E-DIII Flexibility at 40°C

Since the smooth and the bumpy forms of DENV2 do not differ in their infectivity (Fibriansah et al., 2013), we monitored the effect of DENV2 E-DIII large-scale conformational flexibility by measuring infectivity on mammalian BHK21 cells using a plaque assay (Kaufmann and Kabelitz, 2002; Martin, 1978). For this, DENV2 were incubated at 25°C, 37°C, and 40°C to attain the smooth, the partial reversible bumpy, and the irreversible bumpy morphologies, respectively. Interestingly, the number of plaques produced by the irreversible bumpy DENV2 particles (virus incubated at 40°C) was found to be ~3-fold smaller than the number of plaques generated either by the partially reversible bumpy DENV2 (virus incubated at 37°C) or the smooth DENV2 (virus incubated at 25°C) (Figure 5C, gray bars). Since virus aggregation can also lead to reduction in its infectivity, we tested the effect of time-dependent aggregation on DENV2 infectivity (Figure 5D) by incubating viruses at 37°C for up to 2 hr. No significant effect of DENV2 incubation on its infectivity was observed and, thus, the ~3-fold decrease in the number of plaques at 40°C can only be attributed to the loss of DENV2 E-III flexibility. The results are in line with the involvement of E-DIII in the host-receptor binding process (Crill and Roehrig, 2001; Hung et al., 2004; Modis et al., 2003; Rey et al., 1995). The results also indicate that DENV2 E-DIII large-scale conformational flexibility probably plays a role during infectivity of both the smooth and partial bumpy form of DENV2. Moreover, loss of such E-DIII flexibility probably inhibits the interaction of E-DIII with host receptors in the irreversible bumpy DENV2 morphology.

We supported the DENV2 infectivity loss by using DENV2-specific human monoclonal antibody (HMAb) 2D22, which is therapeutic in a mouse model of antibody-enhanced severe dengue disease (de Alwis et al., 2012). HMAb 2D22 binds across DENV2 E proteins in the dimeric structure, and locks E-DIII large-scale conformational changes both before and after DENV2 morphological changes at 37°C (Fibriansah et al., 2015). Thus, HMAb 2D22-bound DENV2 at 37°C should mimic the irreversible bumpy morphology of DENV2, formed due to heating at 40°C, so no changes in DENV2 E-protein conformations should be observed either in the absence or presence of divalent cations.

To achieve this, we added HMAb 2D22 to either the smooth (at 25°C) or bumpy (at 37°C) form of DENV2 in the presence of either Mg^{2+} or Ca^{2+} ions. As expected, no significant changes in the values of the $<\tau_f>$ and α_1 (from mean value of 2.2 ± 0.1 ns and 50% ± 4%, respectively) were recorded with the stepwise increase in temperature from 25°C to 37°C (Figures S6A–S6C), suggesting that HMAb 2D22 can bind to and lock the E-DIII domain in smooth DENV2. Similarly, addition of HMAb 2D22 to

DENV2 at 37°C caused no decrease in the values of the $<\tau_f>$ and α_1 (from mean value of 3.0 ± 0.1 ns and 72% ± 3%, respectively), with the stepwise reversal of temperature from 37°C to 25°C (Figures S6A–S6C). This result indicates that HMAb 2D22 can also bind to and lock the E-DIII domain in the bumpy morphology of DENV2. Taken together, our results indicate that HMAb 2D22 exerted loss of E-DIII large-scale conformational flexibility in both the smooth and bumpy form of DENV2, resulting in a reduction of viral infectivity (de Alwis et al., 2012; Lim et al., 2017a). By analogy, loss of E-DIII large-scale conformational flexibility due to exposure to temperature of 40°C or above may result in the reduction of DENV2 infectivity (Figure 5C, gray bars). However, we are monitoring the overall distance changes between DENV2 E-DIII or DENV1 E-DIII/E-DII to their respective viral bilayers and have limited information about the magnitude of conformational changes undergone at the peptide level. Thus, we cannot exclude the possibility that the overall E-protein conformations could be different in the presence of HMAb 2D22 compared with those at 40°C.

Since infectivity of both the smooth (at 25°C) and bumpy (at 37°C and 40°C) DENV2 morphologies are affected by the loss of DENV2 E-DIII large-scale conformational flexibility, this indicates a limited role of the specific DENV morphologies. This notion is further strengthened by the DENV1 infectivity results. DENV1, like DENV2, shows large-scale morphological expansion but unlike DENV2 does not loose E-protein conformational flexibility after experiencing 40°C. In addition, we observed no or marginal difference in the number of plaques produced (Figure 5C, black bars) by DENV1 in both, either before or after experiencing 40°C conditions.

Although the loss of temperature-dependent DENV2 E-DIII large-scale conformational flexibility is clearly distinguishable at 25°C, the differences between flexible and non-flexible E-DIII either at 37°C or at 40°C are indistinguishable (Figures 5A and 5B). Taking into account the similar DENV2 bumpy morphology both at 37°C and 40°C (Lim et al., 2017b), the ~3-fold difference in DENV2 infectivity cannot be explained (Figure 5C) on the basis of the E-protein large-scale conformational changes. On the other hand, it is equally intriguing that DENV2 infectivity does not change between 25°C and 37°C despite strongly temperature-dependent E-protein large-scale conformational changes (Lim et al., 2017b; Lok et al., 2008; Zhang et al., 2013) (compare gray bars in panel marked "before 40°C heating" in Figure 5C). This implies that large-scale E-protein conformational changes are not correlated with DENV infectivity.

DENV2 Shows Reduced E-DIII Dynamics at 40°C Compared with the Range between 25°C and 37°C

Since the large-scale E-DIII conformational changes that are temperature dependent cannot be the basis of DENV infectivity, we investigated what role is played by DENV intrinsic dynamics at faster time and smaller length scales in viral infectivity. Thus, we investigated the E-protein intrinsic dynamics with respect to the viral bilayer for discrete DENV morphologies that lie between the smooth and bumpy forms of the virus.

To achieve this we used FRET-FCS, which analyzes the fluctuations in FRET efficiency caused by protein conformational fluctuations. FRET-FCS uses the same labeled virus used for trFRET but with much higher time resolution to investigate the intrinsic dynamics on the millisecond timescale. Thus, the labeling with donor and acceptor fulfills two tasks: (1) monitoring of viral morphological changes and (2) measuring the protein dynamics and flexibility. As the fluorescence intensities change when a particle moves through a laser focus, FRET-FCS measures the so-called proximity ratio (*p*), which is a function related to the FRET efficiency (explained in Figure S7A) (Wallace et al., 2000, 2001) and which depends strongly on the separation between donor and acceptor but not on the position of the molecule in the observation volume. Therefore, the correlation function of the proximity ratio *p* (*Gp*) is expected to have contributions mainly from structural dynamics, and minimally from molecular diffusion. In addition, by using *Gp*, rather than fluorescence intensity, we simplify the extraction of intramolecular kinetics or intrinsic dynamics for the correlation function. The approach was calibrated (see Figure S7) and used for DENV measurements. Fitting of *Gp* with a stretched exponential provides an effective relaxation time (τ_p) associated with the correlated motion at smaller length scales, and the stretch parameter (β) describes the heterogeneity of the system. β can vary between 1 (where the system displays normal two-state Arrhenius kinetics, with one discrete energy barrier) and 0 (where there is a continuum of equal energy barriers and the system shows power-law kinetics).

Next, a stepwise increase in temperature from 25°C to 37°C, in either the presence or absence of Mg^{2+} ions, resulted in no or marginal increase in values of τ_p (~0.9 ms) (Figures 6C and 6D) and β (~0.5) (Figures S7C and S7D) for both DENV2 and DENV1. The absence of any changes in intrinsic dynamics is more surprising for DENV2, as it undergoes changes from the smooth to the bumpy form between these two temperatures.

Fitting of DENV2 *Gp* (Figure 6A, blue curve) at 25°C in the presence of Mg^{2+} ions yielded values for τ_p and β of 0.9 ± 0.1 ms (Figure 6C) and 0.48 ± 0.06 (Figure S7C), respectively. In addition, the value obtained for β confirms the DENV2 heterogeneity and existence of more than two E-protein conformational states. Moreover, similar values for τ_p = 0.89 ± 0.1 ms (Figure 6D) and β = 0.5 ± 0.04 (Figure S7D) were obtained for DENV2 E-DIII intrinsic dynamics in the absence of Mg^{2+} ions, suggesting the limited role of divalent cations for protein dynamics in contrast to the morphological changes. Next, fitting of DENV1 *Gp* (Figure 6B) provided values for τ_p (0.9 ± 0.1 ms and 0.9 ± 0.1 ms in presence and absence of Mg^{2+} ions, respectively) and β (0.51 ± 0.04 and 0.51 ± 0.04 in presence and absence of Mg^{2+} ions, respectively) similar to those for DENV2. The similarities in τ_p and β values between DENV2 and DENV1 suggests that both DENV E proteins show similar intrinsic dynamics at smaller length scales.

An increase in temperature from 37°C to 40°C resulted in a ~2.5-fold increase of τ_p for both DENV2 ($2.1 \pm 0.05_{+Mg}$ and $2.3 \pm 0.1_{-Mg}$) and DENV1 ($2.1 \pm 0.05_{+Mg}$ and $2.3 \pm 0.1_{-Mg}$) (Figure 6D), while insignificant changes in β for DENV2 ($0.70 \pm 0.06_{+Mg}$ and $0.61 \pm 0.1_{-Mg}$) and DENV1 ($0.51 \pm 0.02_{+Mg}$ and $0.59 \pm 0.1_{-Mg}$) were observed.

When reversing the temperature from 40°C to 25°C, no change in the values of τ_p (Figures 6C and 6D) was observed for DENV2. This result reveals the correlation between the losses of E-protein flexibility, at high temperature, and the decrease in its intrinsic dynamics. Consequently, this irreversible ~2.5-fold

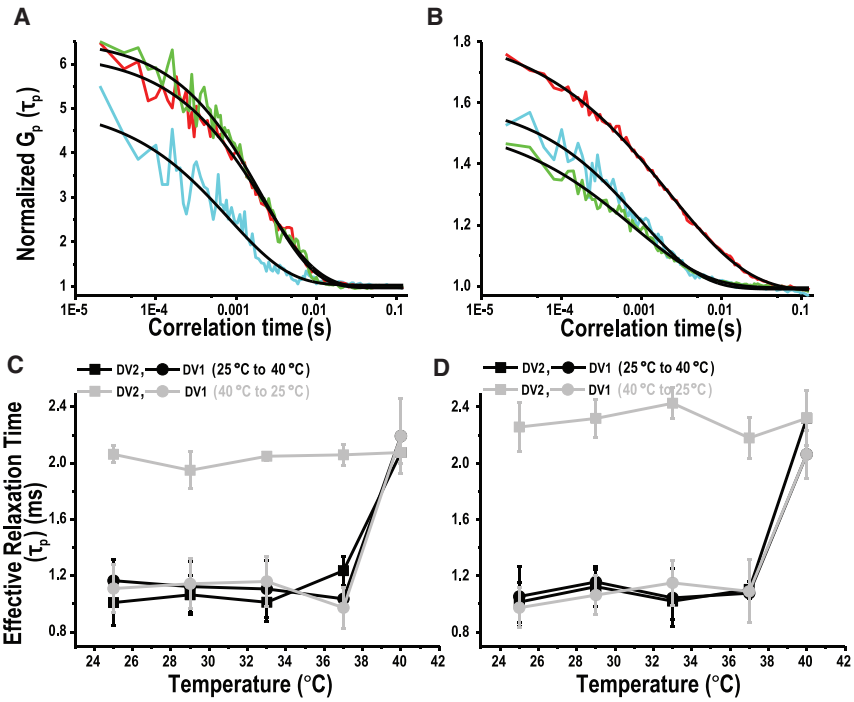

Figure 6. Fluctuation Dynamics of DENV2 and DENV1 between 25°C and 40°C in Absence and Presence of Mg^{2+}

Autocorrelation curves of proximity ratio for (A) 5 × 10^7 PFU/mL DENV2 and (B) 5 × 10^7 PFU/mL DENV1 in the presence of 1 mM Mg^{2+}. Representative curves are plotted at 25°C (cyan traces) after temperature increase from 25°C to 40°C (gray traces) and finally followed by decrease from 40°C to 25°C (green traces). The black line represents the best fit to stretched exponential, and the obtained values are discussed in the article. Effective relaxation time, τ_P, was calculated by fitting these autocorrelation curves of proximity ratio for DENV2 (squares) and DENV1 (circles) either in the presence (C) or absence (D) of 1 mM Mg^{2+}. The data were collected during temperature increase from 25°C to 40°C (black circles/squares) followed by decrease from 40°C to 25°C (gray circles/squares). Error bars represent SDs of four different experimental replicates in both DENV2 and DENV1 viruses, and the values are provided in Table S2.

reduction in DENV2 E-protein intrinsic dynamics in the non-flexible conformation at ≤37°C may be responsible for decreased DENV2 infectivity (Figure 5C). Similarly, the lack of change in DENV2 intrinsic dynamics at 25°C and 37°C (before experiencing 40°C) coincides well with the unchanged DENV2 infectivity in either the smooth or the bumpy morphology (Fibriansah et al., 2013) (Figure 5C). Thus, the results indicate the role of virus intrinsic dynamics as compared with virus morphologies.

This notion was further supported by the reversibility of τ_p (~2.1 ms → ~0.9 ms) for DENV1 (in both the presence [Figure 6C] and absence [Figure 6D] of divalent cations from 40°C → 25°C) that correlates well with unperturbed DENV1 infectivity, even after exposure to 40°C (Figure 5C, black bars). The results indicate that the reversible E-protein intrinsic dynamics (~0.9 ms → ~2.1 ms → ~0.9 ms) may lead to reversible large-scale conformational changes as seen with DENV1 between 37°C and 40°C. Similarly, the unchanged E-protein intrinsic dynamics between 25°C and 37°C, correlate with the unperturbed DENV2 infectivity of the smooth and bumpy forms (Figure 5C). Therefore, DENV E-protein intrinsic dynamics, but not its static conformations, are correlated with viral infectivity and explain the differences in DENV1 and DENV2 infectivity.

Summary

Various dengue virus strains undergo morphological changes from a smooth low-temperature morphology to a bumpy morphology above 35°C. This transition, called "breathing" (Cockburn et al., 2012; Dowd and Pierson, 2011; Lok et al., 2008; Pierson and Diamond, 2012), is similar to the "breathing" effect observed in icosahedral picornaviruses that reversibly expose cleavage sites to proteases (Jimenez et al., 2000; Katpally et al., 2009; Li et al., 1994; Pulli et al., 1998; Witz and Brown, 2001). Thus, by analogy, DENV "breathing" implies some reversible conformational changes of DENV envelope proteins. However, earlier studies showed that heating the smooth low-temperature DENV2 virus to temperatures above 35°C produced an irreversible bumpy morphology that did not change even when reducing the temperature to below 35°C (Fibriansah et al., 2013, 2015; Lim et al., 2017b; Zhang et al., 2013). These studies, however, were conducted in the absence of divalent cations, which could be the reason for the persistence of irreversible viral transitions that would prevent DENV E protein to undergo picornavirus-like reversible large-scale conformational changes. Here, therefore, we demonstrated that the addition of Mg^{2+} or Ca^{2+} ions at physiological concentrations restores a partial reversibility, underlining the importance of divalent cations for viral functionality. However, it should be noted that we observed large-scale conformational changes in only ~15%–20% of DENV. This structural heterogeneity, arising due to incomplete cleavage of precursor to membrane or other perturbations, may help viruses to avoid detection by antibodies (Dowd et al., 2014).

Nevertheless, we were not able to correlate the envelope conformations to infectivity. Large-scale conformational changes in the DENV E protein can be inhibited by using antibodies that can lock the virus in both the smooth and the bumpy morphologies with reduced infectivity. However, unlike the antibody-locked irreversible morphology, the temperature-induced irreversible bumpy DENV2 morphology did not reduce viral infectivity in BHK21 cells (Fibriansah et al., 2013). Furthermore, plaque assays demonstrated that the conformational state of the virus envelope of DENV1 and DENV2 are not correlated with viral infectivity.

We therefore investigated the E-protein intrinsic dynamics at smaller distances and faster time scales, for both smooth and bumpy forms, under the same conditions. The intrinsic dynamics

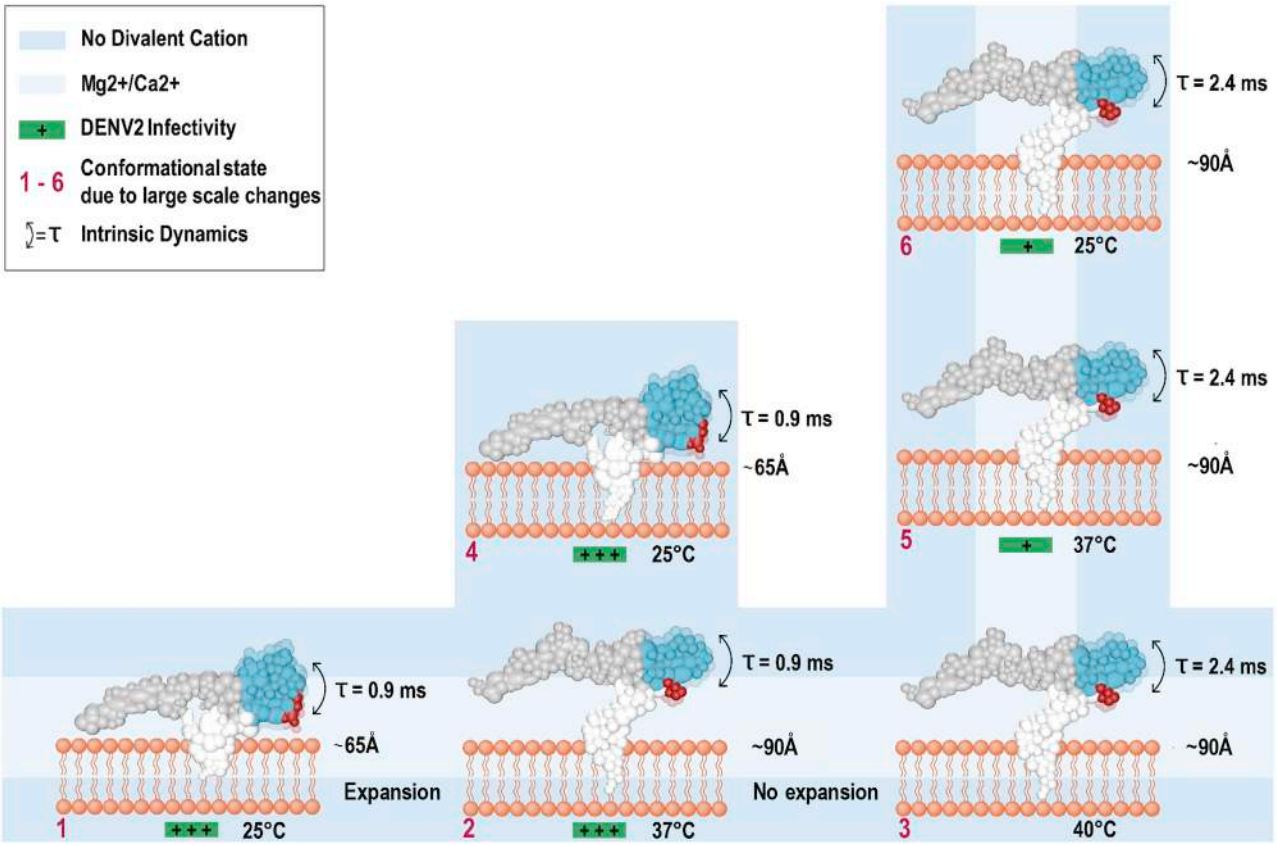

Figure 7. Proposed Model Differentiating Modes of DENV2 "Breathing" and its Correlation with Virus Infectivity

The diagram summarizes divalent cation- and temperature-dependent large- and small-scale changes in DENV2 E-DIII at 5-fold vertex. (1) In smooth virus (PDB: 3J27), E-DIII is buried in pentameric units at an average distance of ~65 Å from the viral bilayer and shows intrinsic dynamics in ~0.9-ms range. During viral expansion (PDB: 3ZKO), both in the presence (blue color) and absence (light blue color) of divalent cations, up to either (2) 37°C or (3) 40°C, E-DIII undergoes large-scale conformational changes and the average distance increases to ~90 Å from 65 Å, but shows intrinsic dynamics in ~0.9-ms and ~2.4-ms range at 37°C and 40°C, respectively. (4) E-DIII undergoes temperature-dependent large-scale conformational contraction only in the presence of divalent cations, with lowering of temperature from 37°C to 25°C. The average distance between E-DIII and bilayer decreased from ~90 Å to 65 Å. When heated to 40°C and lowering of temperature either to (5) 37°C or (6) 25°C, E-DIII loses its ability to undergo large-scale temperature-dependent conformational changes and thus, no change in either distance between E-DIII with respect to bilayer or domain-intrinsic dynamics are observed. Under such conditions, DENV2 shows reduced infectivity (plus signs on green background) in BHK21 cells.

measured by FRET-FCS indicated that for DENV1 E protein the intrinsic dynamics as well as infectivity did not change between 25°C and 40°C. DENV2 E protein, however, showed a 2.5-fold decrease in intrinsic dynamics at 40°C compared with the dynamics between 25°C and 37°C, and also showed a concomitant decrease in infectivity (Figure 7).

This work on the large-scale conformational changes and intrinsic dynamics of DENV E proteins shows a remarkable adaptation of the virus to its two hosts' temperatures to attain infectivity. It shows not only the importance of divalent cations for the structural and dynamic investigation of viruses, but also demonstrates that measuring dynamics complements the DENV structural studies and is critical for determining factors influencing DENV infectivity. These dynamic events are essential aspects of the DENV life cycle and could be targeted in antiviral strategies. Lastly, we speculate that mutations targeting DENV intrinsic dynamics instead of large-scale conformational changes may be instrumental in producing attenuated viruses that are capable of invoking neutralizing antibodies.

STAR★METHODS

Detailed methods are provided in the online version of this paper and include the following:

- KEY RESOURCES TABLE
- CONTACT FOR REAGENT AND RESOURCE SHARING
- EXPERIMENTAL MODEL AND SUBJECT DETAILS
  - Cell Lines
  - Dyes and Viruses
- METHOD DETAILS
  - Virus Labeling
  - Plaque-Forming Assay
  - Time Resolved Förster Resonance Energy Transfer (trFRET) Measurements
  - Identification of Biotin-Labelled Sites on DENV2 Proteins
  - Reversibility of DENV2 Expansion in the Presence and Absence of Mg^{2+} by HDXMS

SUPPLEMENTAL INFORMATION

Supplemental Information includes seven figures and five tables and can be found with this article online at https://doi.org/10.1016/j.str.2018.12.006.

ACKNOWLEDGMENTS

K.K.S., X.-X.L., S.N.T., A.G., J.K.M., X.Y.E.L., G.S.A., and T.W. were supported by a Singapore Ministry of Education Tier 3 grant (MOE2012-T3-1-008). We are thankful to Sonia Monti for helping in the preparation of the figures.

AUTHOR CONTRIBUTIONS

K.K.S. and T.W. designed, analyzed, and interpreted the results. X.-X.L. performed the HDXMS experiments. K.K.S. and T.W. performed the trFRET and FRET-FCS experiments and wrote the section on trFRET and FRET-FCS. S.N.T. performed plaque assay. A.G. wrote software for FRET-FCS analysis. J.K.M. and P.J.B. provided computational data. X.Y.E.L. provided virus samples. K.K.S. and T.W. wrote the manuscript and D.H., G.S.A., K.K.S., T.W., and P.J.B. contributed to manuscript revision.

DECLARATION OF INTERESTS

The authors declare no competing interests.

Received: May 23, 2018
Revised: October 2, 2018
Accepted: December 9, 2018
Published: January 24, 2019

REFERENCES

Bennett, S.N., Campbell, A.D., Hancock, A., Johnstone, C., Kenny, P.W., Pickup, A., Plowright, A.T., Selmi, N., Simpson, I., et al. (2010). Discovery of a series of indan carboxylic acid glycogen phosphorylase inhibitors. Bioorg. Med. Chem. Lett. *20*, 3511–3514.

Best, R.B., Zhu, X., Shim, J., Lopes, P.E., Mittal, J., Feig, M., Mackerell, A.D., Jr., et al. (2012). Optimization of the additive CHARMM all-atom protein force field targeting improved sampling of the backbone phi, psi and side-chain chi(1) and chi(2) dihedral angles. J. Chem. Theory Comput. *8*, 3257–3273.

Bhatt, S., Gething, P.W., Brady, O.J., Messina, J.P., Farlow, A.W., Moyes, C.L., Drake, J.M., Brownstein, J.S., Hoen, A.G., Sankoh, O., et al. (2013). The global distribution and burden of dengue. Nature *496*, 504–507.

Bond, P.J., Holyoake, J., Ivetac, A., Khalid, S., Sansom, M.S., et al. (2007). Coarse-grained molecular dynamics simulations of membrane proteins and peptides. J. Struct. Biol. *157*, 593–605.

Butrapet, S., Childers, T., Moss, K.J., Erb, S.M., Luy, B.E., Calvert, A.E., Blair, C.D., Roehrig, J.T., Huang, C.Y., et al. (2011). Amino acid changes within the E protein hinge region that affect dengue virus type 2 infectivity and fusion. Virology *413*, 118–127.

Cockburn, J.J., Navarro Sanchez, M.E., Fretes, N., Urvoas, A., Staropoli, I., Kikuti, C.M., Coffey, L.L., Arenzana Seisdedos, F., Bedouelle, H., Rey, F.A., et al. (2012). Mechanism of dengue virus broad cross-neutralization by a monoclonal antibody. Structure *20*, 303–314.

Cotmore, S.F., Hafenstein, S., Tattersall, P., et al. (2010). Depletion of virion-associated divalent cations induces parvovirus minute virus of mice to eject its genome in a 3′-to-5′ direction from an otherwise intact viral particle. J. Virol. *84*, 1945–1956.

Crill, W.D., and Roehrig, J.T. (2001). Monoclonal antibodies that bind to domain III of dengue virus E glycoprotein are the most efficient blockers of virus adsorption to Vero cells. J. Virol. *75*, 7769–7773.

de Alwis, R., Smith, S.A., Olivarez, N.P., Messer, W.B., Huynh, J.P., Wahala, W.M., White, L.J., Diamond, M.S., Baric, R.S., Crowe, J.E., Jr., et al. (2012). Identification of human neutralizing antibodies that bind to complex epitopes on dengue virions. Proc. Natl. Acad. Sci. U S A *109*, 7439–7444.

Dowd, K.A., Mukherjee, S., Kuhn, R.J., Pierson, T.C., et al. (2014). Combined effects of the structural heterogeneity and dynamics of flaviviruses on antibody recognition. J. Virol. *88*, 11726–11737.

Dowd, K.A., and Pierson, T.C. (2011). Antibody-mediated neutralization of flaviviruses: a reductionist view. Virology *411*, 306–315.

Dror, R.O., Jensen, M.Ø., Borhani, D.W., Shaw, D.E., et al. (2010). Exploring atomic resolution physiology on a femtosecond to millisecond timescale using molecular dynamics simulations. J. Gen. Physiol. *135*, 555–562.

Englander, S.W., and Kallenbach, N.R. (1983). Hydrogen exchange and structural dynamics of proteins and nucleic acids. Q. Rev. Biophys. *16*, 521–655.

Fibriansah, G., Ibarra, K.D., Ng, T.S., Smith, S.A., Tan, J.L., Lim, X.N., Ooi, J.S., Kostyuchenko, V.A., Wang, J., de Silva, A.M., et al. (2015). DENGUE VIRUS. Cryo-EM structure of an antibody that neutralizes dengue virus type 2 by locking E protein dimers. Science *349*, 88–91.

Fibriansah, G., Ng, T.S., Kostyuchenko, V.A., Lee, J., Lee, S., Wang, J., Lok, S.M., et al. (2013). Structural changes in dengue virus when exposed to a temperature of 37 degrees C. J. Virol. *87*, 7585–7592.

Gallichotte, E.N., Dinnon, K.H., 3rd, Lim, X.N., Ng, T.S., Lim, E.X.Y., Menachery, V.D., Lok, S.M., Baric, R.S., et al. (2017). CD-loop extension in Zika virus envelope protein key for stability and pathogenesis. J. Infect. Dis. *216*, 1196–1204.

Gubler, D.J. (2002). Epidemic dengue/dengue hemorrhagic fever as a public health, social and economic problem in the 21st century. Trends Microbiol. *10*, 100–103.

Gubler, D.J. (2012). The economic burden of dengue. Am. J. Trop. Med. Hyg. *86*, 743–744.

Guzman, M.G., Halstead, S.B., Artsob, H., Buchy, P., Farrar, J., Gubler, D.J., Hunsperger, E., Kroeger, A., Margolis, H.S., Martínez, E., et al. (2010). Dengue: a continuing global threat. Nat. Rev. Microbiol. *8*, S7–S16.

Haas, E., Katchalski-Katzir, E., Steinberg, I.Z., et al. (1978). Effect of the orientation of donor and acceptor on the probability of energy transfer involving electronic transitions of mixed polarization. Biochemistry *17*, 5064–5070.

Halstead, S.B. (2012a). Controversies in dengue pathogenesis. Paediatr. Int. Child Health *32* (*Suppl 1*), 5–9.

Halstead, S.B. (2012b). Dengue vaccine development: a 75% solution? Lancet *380*, 1535–1536.

Halstead, S.B. (2013). Dengue vascular permeability syndrome: what, no T cells? Clin. Infect. Dis. *56*, 900–901.

Holmes, E.C. (2003). Patterns of intra- and interhost nonsynonymous variation reveal strong purifying selection in dengue virus. J. Virol. *77*, 11296–11298.

Hung, J.J., Hsieh, M.T., Young, M.J., Kao, C.L., King, C.C., Chang, W., et al. (2004). An external loop region of domain III of dengue virus type 2 envelope protein is involved in serotype-specific binding to mosquito but not mammalian cells. J. Virol. *78*, 378–388.

Jimenez, R., Barniol, R., de Barniol, L., Machuca, M., et al. (2000). Periodic occurrence of epithelial viral necrosis outbreaks in *Penaeus vannamei* in Ecuador. Dis. Aquat. Organ. *42*, 91–99.

Jo, S., Kim, T., Iyer, V.G., Im, W., et al. (2008). CHARMM-GUI: a web-based graphical user interface for CHARMM. J. Comput. Chem. *29*, 1859–1865.

Katpally, U., Fu, T.M., Freed, D.C., Casimiro, D.R., Smith, T.J., et al. (2009). Antibodies to the buried N terminus of rhinovirus VP4 exhibit cross-serotypic neutralization. J. Virol. *83*, 7040–7048.

Kaufmann, S.H., and Kabelitz, D. (2002). Methods in Microbiology: Immunology of Infection, *Vol 32* (Academic Press).

Klauda, J.B., Venable, R.M., Freites, J.A., O'Connor, J.W., Tobias, D.J., Mondragon-Ramirez, C., Vorobyov, I., MacKerell, A.D., Jr., Pastor, R.W., et al. (2010). Update of the CHARMM all-atom additive force field for lipids: validation on six lipid types. J. Phys. Chem. B *114*, 7830–7843.

Kostyuchenko, V.A., Chew, P.L., Ng, T.S., Lok, S.M., et al. (2014). Near-atomic resolution cryo-electron microscopic structure of dengue serotype 4 virus. J. Virol. *88*, 477–482.

Kruse, J., Krüse, K.M., Witz, J., Chauvin, C., Jacrot, B., Tardieu, A., et al. (1982). Divalent ion-dependent reversible swelling of tomato bushy stunt virus and organization of the expanded virion. J. Mol. Biol. *162*, 393–414.

Kudlacek, S.T., Premkumar, L., Metz, S.W., Tripathy, A., Bobkov, A.A., Payne, A.M., Graham, S., Brackbill, J.A., Miley, M.J., de Silva, A.M., et al. (2018). Physiological temperatures reduce dimerization of dengue and Zika virus recombinant envelope proteins. J. Biol. Chem. *293*, 8922–8933.

Kuhn, R.J., Zhang, W., Rossmann, M.G., Pletnev, S.V., Corver, J., Lenches, E., Jones, C.T., Mukhopadhyay, S., Chipman, P.R., Strauss, E.G., et al. (2002). Structure of dengue virus: implications for flavivirus organization, maturation, and fusion. Cell *108*, 717–725.

Kyle, J.L., and Harris, E. (2008). Global spread and persistence of dengue. Annu. Rev. Microbiol. *62*, 71–92.

Li, Q., Yafal, A.G., Lee, Y.M., Hogle, J., Chow, M., et al. (1994). Poliovirus neutralization by antibodies to internal epitopes of VP4 and VP1 results from reversible exposure of these sequences at physiological temperature. J. Virol. *68*, 3965–3970.

Lim, X.X., Chandramohan, A., Lim, X.E., Crowe, J.E., Jr., Lok, S.M., Anand, G.S., et al. (2017a). Epitope and paratope mapping reveals temperature-dependent alterations in the dengue-antibody interface. Structure *25*, 1391–1402.e3.

Lim, X.X., Chandramohan, A., Lim, X.Y., Bag, N., Sharma, K.K., Wirawan, M., Wohland, T., Lok, S.M., Anand, G.S., et al. (2017b). Conformational changes in intact dengue virus reveal serotype-specific expansion. Nat. Commun. *8*, 14339.

Lok, S.M., Kostyuchenko, V., Nybakken, G.E., Holdaway, H.A., Battisti, A.J., Sukupolvi-Petty, S., Sedlak, D., Fremont, D.H., Chipman, P.R., Roehrig, J.T., et al. (2008). Binding of a neutralizing antibody to dengue virus alters the arrangement of surface glycoproteins. Nat. Struct. Mol. Biol. *15*, 312–317.

Marrink, S.J., Risselada, H.J., Yefomov, S., Tieleman, D.P., and de Vries, A.H. (2007). The MARTINI force field: coarse grained model for biomolecular simulations. J. Phys. Chem. B *111*, 7812–7824.

Martin, S.J. (1978). The Biochemistry of Viruses (Cambridge University Press).

Messer, W.B., de Alwis, R., Yount, B.L., Royal, S.R., Huynh, J.P., Smith, S.A., Crowe, J.E., Jr., Doranz, B.J., Kahle, K.M., Pfaff, J.M., et al. (2014). Dengue virus envelope protein domain I/II hinge determines long-lived serotype-specific dengue immunity. Proc. Natl. Acad. Sci. U S A. *111*, 1939–1944.

Modis, Y., Ogata, S., Clements, D., Harrison, S.C., et al. (2003). A ligand-binding pocket in the dengue virus envelope glycoprotein. Proc. Natl. Acad. Sci. U S A *100*, 6986–6991.

Morens, D.M., and Fauci, A.S. (2008). Dengue and hemorrhagic fever: a potential threat to public health in the United States. JAMA *299*, 214–216.

Mukhopadhyay, S., Kuhn, R.J., Rossmann, M.G., et al. (2005). A structural perspective of the flavivirus life cycle. Nat. Rev. Microbiol. *3*, 13–22.

Perilla, J.R., Goh, B.C., Cassidy, C.K., Liu, B., Bernardi, R.C., Rudack, T., Yu, H., Wu, Z., Schulten, K., et al. (2015). Molecular dynamics simulations of large macromolecular complexes. Curr. Opin. Struct. Biol. *31*, 64–74.

Pierson, T.C., and Diamond, M.S. (2012). Degrees of maturity: the complex structure and biology of flaviviruses. Curr. Opin. Virol. *2*, 168–175.

Pulli, T., Roivainen, M., Hovi, T., Hyypiä, T., et al. (1998). Induction of neutralizing antibodies by synthetic peptides representing the C terminus of coxsackievirus A9 capsid protein VP1. J. Gen. Virol. *79* (Pt 9), 2249–2253.

Reddy, S.V., Reddy, K.T., Kumari, V.V., Basha, S.H., et al. (2015). Molecular docking and dynamic simulation studies evidenced plausible immunotherapeutic anticancer property by Withaferin A targeting indoleamine 2,3-dioxygenase. J. Biomol. Struct. Dyn. *33*, 2695–2709.

Rey, F.A. (2013). Dengue virus: two hosts, two structures. Nature *497*, 443–444.

Rey, F.A., Heinz, F.X., Mandl, C., Kunz, C., Harrison, S.C., et al. (1995). The envelope glycoprotein from tick-borne encephalitis virus at 2 A resolution. Nature *375*, 291–298.

Sabchareon, A., Sirivichayakul, C., Limkittikul, K., Chanthavanich, P., Suvannadabba, S., Jiwariyavej, V., Dulyachai, W., Pengsaa, K., Margolis, H.S., Letson, G.W., et al. (2012). Dengue infection in children in Ratchaburi, Thailand: a cohort study. I. Epidemiology of symptomatic acute dengue infection in children, 2006-2009. PLoS Negl. Trop. Dis. *6*, e1732.

Sherman, M.B., Guenther, R.H., Tama, F., Sit, T.L., Brooks, C.L., Mikhailov, A.M., Orlova, E.V., Baker, T.S., Lommel, S.A., et al. (2006). Removal of divalent cations induces structural transitions in red clover necrotic mosaic virus, revealing a potential mechanism for RNA release. J. Virol. *80*, 10395–10406.

Shirley, J.A., Beards, G.M., Thouless, M.E., Flewett, T.H., et al. (1981). The influence of divalent cations on the stability of human rotavirus. Arch. Virol. *67*, 1–9.

Van Der Spoel, D., Lindahl, E., Hess, B., Groenhof, G., Mark, A.E., Berendsen, H.J., et al. (2005). GROMACS: fast, flexible, and free. J. Comput. Chem. *26*, 1701–1718.

Wales, T.E., and Engen, J.R. (2006). Hydrogen exchange mass spectrometry for the analysis of protein dynamics. Mass Spectrom. Rev. *25*, 158–170.

Wallace, M.I., Ying, L., Balasubramanian, S., Klenerman, D., et al. (2001). Non-Arrhenius kinetics for the loop closure of a DNA hairpin. Proc. Natl. Acad. Sci. U S A *98*, 5584–5589.

Wallace, M.I., Ying, L.M., et al. (2000). FRET fluctuation spectroscopy: exploring the conformational dynamics of a DNA hairpin loop. J. Phys. Chem. B *104*, 11551–11555.

Witz, J., and Brown, F. (2001). Structural dynamics, an intrinsic property of viral capsids. Arch. Virol. *146*, 2263–2274.

Woodward, C., Simon, I., Tüchsen, E., et al. (1982). Hydrogen exchange and the dynamic structure of proteins. Mol. Cell. Biochem. *48*, 135–160.

Zhang, Q., Hunke, C., Yau, Y.H., Seow, V., Lee, S., Tanner, L.B., Guan, X.L., Wenk, M.R., Fibriansah, G., Chew, P.L., et al. (2012). The stem region of premembrane protein plays an important role in the virus surface protein rearrangement during dengue maturation. J. Biol. Chem. *287*, 40525–40534.

Zhang, X., Sheng, J., Plevka, P., Kuhn, R.J., Diamond, M.S., Rossmann, M.G., et al. (2013). Dengue structure differs at the temperatures of its human and mosquito hosts. Proc. Natl. Acad. Sci. U S A *110*, 6795–6799.

Zhang, X., Sun, L., Rossmann, M.G., et al. (2015). Temperature dependent conformational change of dengue virus. Curr. Opin. Virol. *12*, 109–112.

Zhang, Z., and Smith, D.L. (1993). Determination of amide hydrogen exchange by mass spectrometry: a new tool for protein structure elucidation. Protein Sci. *2*, 522–531.

Zhao, C., Zhang, B., and Du, W. (2013). Effects of distal mutation on the dynamic properties of carboxycytoglobin: a molecular dynamics simulation study. J. Biol. Inorg. Chem. *18*, 947–955.

STAR★METHODS

KEY RESOURCES TABLE

REAGENT or RESOURCE	SOURCE	IDENTIFIER
Antibodies		
Fab fragment of 2D22	de Alwis et al., 2012	N/A
Bacterial and Virus Strains		
DENV2 New Guinea C strain (NGC)	The laboratory of Michael Rossmann	N/A
DENV1 PVP 159 strain	The laboratory of Michael Rossmann	N/A
Chemicals, Peptides, and Recombinant Proteins		
HEPES (Hyclone)	GE Healthcare life sciences	SH30237.01
NaCl	Sigma-Aldrich	7647-14-5
Alexa 488 TFP ester	Invitrogen	
1,1'-Dioctadecyl-3,3,3',3'-Tetramethylindocarbocyanine Perchlorate (DiI-C18)	Invitrogen	
TrisHCl	Sigma-Aldrich	185-53-1
NaCl	Sigma-Aldrich	7647-14-5
EDTA	Sigma-Aldrich	60-00-4
bovine serum albumin (BSA)	Sigma-Aldrich	9048-46-8
D_2O	Cambridge Isotope Laboratory Inc.	7789-20-0
NaOH	Sigma-Aldrich	1310-73-2
GnHCl	Sigma-Aldrich	50-01-1
Tris(2-carboxyethyl) phosphine-hydrochloride (TCEP-HCl)	Sigma-Aldrich	51805-45-9
titanium dioxide (TiO_2)	Sigma-Aldrich	13463-67-7
RPMI (Roswell Park Memorial Institute)	Sigma-Aldrich	R8758
$MgCl_2$	Sigma-Aldrich	CAS 7791-18-6
Experimental Models: Cell Lines		
C6/36 Aedes albopitus mosquito cells	American Type Culture Collection (ATCC)	CRL-1660
baby hamster kidney fibroblast cells (BHK 21)	American Type Culture Collection (ATCC)	CCL-10
Oligonucleotides		
5'-GGGTT-$(A)_{30}$-AACCC-3'	Wallace et al., 2001, IDT	N/A
Software and Algorithms		
Origin 9.1	Origin labs	https://www.originlab.com/demodownload.aspx
PROTEIN LYNX GLOBAL SERVER version 3.0	Waters	http://www.waters.com/waters/en_SG/ProteinLynx-Global-SERVER
DYNAMX Ver. 2.0 software	Waters	http://www.waters.com/waters/library.htm?cid=511436&lid=134832928&locale=en_SG
GROMACS 5.1.4 package	Van Der Spoel et al., 2005	http://manual.gromacs.org/documentation/5.1.4/index.html
Chimera	Resource for Biocomputing, Visualization, and Informatics (RBVI)	https://www.cgl.ucsf.edu/chimera/

CONTACT FOR REAGENT AND RESOURCE SHARING

Further information and requests for resources and reagents should be directed to and will be fulfilled by the corresponding author, Thorsten Wohland (twohland@nus.edu.sg).

EXPERIMENTAL MODEL AND SUBJECT DETAILS

Cell Lines

C6/36 mosquito cells and baby hamster kidney strain 21 (BHK21) fibroblast cells were from the American Type culture collection (ATCC). C6/36 were cells derived from larvae of female *Aedes albopictus* (*skuse*) mosquito and were adapted to Eagle's minimum essential medium. Cells were then cloned and recloned by seeding single cell suspensions into petri dishes. BHK21 cells were derived from baby hamster kidneys of five unsexed, 1-day-old hamsters (*Mesocricetus auratus*). Further information about the cells lines can be obtained through Key Resources Table.

Dyes and Viruses

Both alexafluor 488 TFP ester (AF488-TFP) and 1,1'-Dioctadecyl-3,3,3',3'-Tetramethylindocarbocyanine Perchlorate (DiI-C18) were purchased from Invitrogen (Singapore). DENV2 NGC and DENV1 PVP159 were produced and purified as previously described (Fibriansah et al., 2013; Lim et al., 2017b).

METHOD DETAILS

Virus Labeling

Alexa Fluor 488 TFP ester (AF488-TFP) and 1,1′-Dioctadecyl-3,3,3′,3′-Tetramethylindocarbocyanine Perchlorate (DiI-C18) were purchased from ThermoFisher Scientific, Singapore. Purified viruses had stock concentrations of 6×10^{10} plaque forming units (PFU)/ml for DENV2 (NGC) and 4.2×10^{10} PFU/ml for DENV1 (PVP 159). Both DENV1 (PVP 159) and DENV2 (NGC) were dual labelled by sequential addition of DiI-C18 and AF488-TFP, in buffer containing 10 mM HEPES, 150 mM NaCl at pH 7.4 (HN buffer). The DiI-C18 and AF488-TFP stock solutions were prepared in dimethylsulfoxide and subsequently their concentrations were determined using molar extinction coefficients of 144,000 $M^{-1}cm^{-1}$ and 71,000 $M^{-1}cm^{-1}$, respectively. Initially, the DiI-C18 stock solution was diluted in 50 μl of HN buffer to a final concentration of 50 nM and sonicated for 10 min. Next, $\sim 2.5 \times 10^8$ PFU of the purified viruses were directly added to the DiI-C18 containing HN buffer solution and incubated for 1 h at 4°C to label the virus-lipid bilayer. Subsequently, AF488-TFP at a final concentration of 750 nM was added to the DiI-C18 labelled virus HN buffer mixture and incubated for an additional hour at room temperature. The free dye molecules were removed by gel filtration (MicroSpinTM S-200 HR columns, GE Healthcare, Singapore). As a control, single labelled donor-only viruses were prepared by labelling with AF488-TFP only.

Plaque-Forming Assay

BHK21 cells were cultured in RPMI supplemented with 10% FBS at 37°C in 5% CO_2. When cells reached approximately 80% confluence, virus infection was carried out. Virus was serially diluted 10-fold from $1:10^2$ to $1:10^{10}$ using RPMI supplemented with 10% FBS. For the experiment, the virus was preincubated at 37°C or 40°C for 30 min and then 100 μl of virus was layered onto the BHK cells, which were preequilibrated at 37°C for 2 h. The cells were then further incubated at their respective temperatures for 2 h. The infected cells were overlaid with RPMI supplemented with 10% FBS and 1% Aquacide. The plates were further incubated at 37°C in 5% CO_2 for 6 days. The cells were then stained by first discarding the supernatant and then adding 1 ml of 0.5% (wt/vol) crystal violet–25% formaldehyde to the cell monolayer and further incubated for 1 h. The cell monolayers were then washed with water, and plaques were counted by visual inspection. The experiments were repeated at least thrice.

Time Resolved Förster Resonance Energy Transfer (trFRET) Measurements

tr-FRET measurements were carried out on a commercial Olympus FV1200 laser scanning confocal microscope (IX83, Olympus, Singapore) equipped with a time-resolved LSM upgrade kit (Microtime 200, PicoQuant, GmbH, Berlin, Germany). The samples were excited with a 485 nm pulsed diode laser with a 20 MHz repetition rate and 29 μW power (PDL series, Sepia II combiner module). The beam was focused into the sample by a water immersion objective (× 60, NA 1.2; Olympus, Tokyo, Japan) after being reflected by a dichroic mirror (DM405/485/543/635 band pass, Olympus, Singapore) and the scanning unit. The fluorescence was collected by the same objective followed by a pinhole (120 μm) to remove out-of-focus light. The fluorescence signal was spectrally divided into donor (green) and acceptor (red) channels by a 560DCLP dichroic mirror. The donor fluorescence was recorded by a set of single molecule avalanche photodiodes (SPADs) (SPCM-AQR-14, PerkinElmer Optoelectronics, Quebec, Canada), through a 520/35 band pass emission filter (Omega, VT). This donor signal was further processed by a time correlated single photon counting card (TimeHarp 260, PicoQuant) to build up the histogram of photon arrival times.

The temperature of the sample was controlled by an on-stage incubator (TempControl 37-2 digital, Pecon, Erbach, Germany) and an objective heater (TC-124A, Warner Instruments, Hamden, CT). The TR-FRET measurements were recorded for 180 s after incubating single/dual-labelled virus samples for at least 30 min, at a given temperature. The mean lifetime angle (τ) was calculated from the individual fluorescence lifetimes (τ_i) and their relative amplitudes (α_i) according to $(\tau)=\Sigma\alpha_i\tau_i$. Donor fluorescence lifetime decay data were treated using the software SymPhoTime 64 (PicoQuant, GmbH). In all cases, the χ^2 values were close to 1 and the weighted residuals as well as their autocorrelation were distributed randomly around 0, indicating a good fit. The reported values are mean and s.d.'s from six replicates for both DENV1 (PVP 159) and DENV2 (NGC) from 3 different purified virus batches.

Identification of Biotin-Labelled Sites on DENV2 Proteins

The C, E and M-proteins from biotin-labelled DENV1 and 2 particles were separated by SDS PAGE analysis. The protein bands were excised from the SDS-PAGE gel and cut into fine bits after fixation with 50% Methanol containing 12% Acetic acid for 30 min at room temperature. Finely-cut gels were washed with 50 mM NH_4HCO_3 in 50% acetonitrile and dehydrated with 100% acetonitrile. Cysteines in the sample were reduced by treatment with 5 mM TCEP (Tris (2-carboxyethyl) phosphine) in 100 mM NH_4HCO_3 for 60 min at 57°C and alkylated with 10 mM MMTS in 100 mM NH_4HCO_3. The protein bands were digested with trypsin (12.5 ng/μL trypsin in 500 mM TEAB (Triethylammonium bicarbonate)) overnight at 37°C. Trypsin fragmentation peptides were eluted from the gel bits using 50 mM TEAB and desalted using Sep-Pak® tC_{18} μElution Plate (186002318, Waters Corp., Milford, MA). The peptides were lyophilized and resuspended in PBS buffer. The biotinylated peptides were affinity purified using immobilized Neutravidin beads (Thermo Fisher Scientific) and the bound biotinylated peptides were eluted with 0.2% trifluoro-acetic acid, 0.1% formic acid in 80% acetonitrile. Eluted peptides were lyophilized and resuspended in PBS buffer before mass spectrometric analysis.

Peptide identification was by an online LC MS/MS using TripleTOF 5600 system (AB SCIEX, Foster City, CA) in Information Dependent Acquisition Mode. The raw mass spectra were identified by searching against the DENV structural proteins database containing amino acid sequences of the C-, E- and M-proteins using the ProteinPilot 4.5 software (July 2012, AB SCIEX) that included variable modification (size-226.0776 Da) on lysine residues.

Reversibility of DENV2 Expansion in the Presence and Absence of Mg^{2+} by HDXMS

HDXMS captures thermodynamic transitions of proteins by measuring the differences in mass when backbone amide hydrogens exchange with solvent deuterium (Wales and Engen, 2006; Zhang and Smith, 1993). The extent of HDX is dependent on hydrogen bonding and solvent accessibility of the protein (Englander and Kallenbach, 1983; Woodward et al., 1982), at the second and slower time scales (Englander and Kallenbach, 1983). Purified DENV2 particles (0.25 mg/mL of E-protein) in NTE buffer were incubated at 28°C and 37°C for 30 min as described (Lim et al., 2017b). In order to assess the reversibility of DENV2 expansion, DENV2 particles were first incubated at 28°C for 30 min and expanded by incubation at 37°C for 30 min followed by incubation at 28°C for 30 min. To test the reversibility of temperature-dependent DENV2 expansion in the presence of Mg^{2+} ions, the DENV2 particles that were pre-incubated in NTE buffer containing 1mM of Mg^{2+}, were subjected to similar temperature perturbations.

Amide Hydrogen/Deuterium Exchange Mass Spectrometry (HDXMS)

The deuterium exchange of DENV2 under the various specified temperature and Mg^{2+} ions conditions were initiated by a 10-fold dilution in the respective buffers that were reconstituted with 99.9% D_2O resulting in 89.9% final D2O concentration. Deuterium exchange under these various conditions were carried for 1 min.

All deuterium exchange reactions were quenched by lowering the pH read to 2.5 upon addition of pre-chilled NaOH in GnHCl and Tris(2-carboxyethyl) phosphine-hydrochloride (TCEP-HCl) to achieve a final concentration of 1.5 M GnHCl and 0.25 M TCEP-HCl. Quenched reactions were maintained at 4°C on ice to minimize back exchange. Viral membrane phospholipids in the DENV2 complexes were removed by adding 0.1 mg of titanium dioxide (TiO_2) (Sigma Aldrich, St. Louis, MO) to the quenched mixture and incubated for 1 min with mixing every 30 s. TiO_2 in the samples were removed with a 0.22 μm filter (Merck Millipore, Darmstadt, Germany) after 1 min of centrifugation at 13,000 rpm. All deuterium exchange reactions were performed in triplicate, and the reported values for every peptide are an average of three independent reactions without correcting for back exchange.

Pepsin Fragment Peptide Identification

Peptides of C-, E- and M-protein from DENV2 NGC were identified by searching the mass spectra of the undeuterated samples of purified DENV2 NGC against DENV2 NGC structural protein database containing amino acid sequences of the C-, E- and M-proteins using PROTEIN LYNX GLOBAL SERVER version 3.0 (Waters, Milford, MA) software. Mass spectra of peptides from a single undeuterated DENV2 NGC samples with precursor ion mass tolerance of <10 ppm, and products per amino acids of at least 0.2 with a minimum intensity of 5000 for both precursor and product ions were selected. Five undeuterated samples were collected and the final peptide list generated from peptides identified independently in at least 2 of the 3 undeuterated samples.

Measurements of Deuterium Uptake and Calculation of Deuterium Exchange Differences

Deuterium uptake of each peptide were measured using DYNAMX Ver. 2.0 software (Waters, Milford, MA) by subtracting the average mass centroid of the peptide after 1 min of deuterium exchange with the average mass centroid of the corresponding undeuterated peptide. Differences in deuterium exchange for all peptides in DENV2 under the various temperature and Mg^{2+} perturbations were determined by subtracting centroid masses of deuterated peptides between two experimental conditions. Deuterium exchange differences from DENV2 E-proteins and displayed from N to C-terminus in the difference plot. The standard deviations for deuterium uptake in all peptides were determined and a difference of 0.5 Da was used as the significance threshold for any differences in deuterium uptake across the two states compared and agrees with the observed standard errors measured in deuterated peptides.

Molecular Dynamics Simulations

Only low-resolution cryo-EM data are available for the "bumpy" expanded state of DENV2, with stem/transmembrane regions of E and M proteins absent. Therefore, a targeted MD (TMD) approach was used to drive a complete, high-resolution structure of the mature "smooth" DENV2 virion (PDB ID: 3J27(Zhang et al., 2013)) towards a structure (PDB ID: 3ZKO(Fibriansah et al., 2013)) of

the expanded virion. During TMD, steering forces were applied in the form of a harmonic potential that is dependent upon the gradient of the root mean squared deviation (RMSD) from the target structure[3]. The initial coordinates for mature DENV2, consisting of 180 E and M proteins embedded within a lipid bilayer, were taken from our previous work.[4] The fully solvated and equilibrated virion system was treated in a coarse-grained (CG) MARTINI (Marrink et al., 2007) representation. Subsequently, the E protein ectodomain structure was biased towards that of the expanded state during TMD.

Following TMD, a single pentamer surrounding a 5-fold vertex of the expanded virion was back-mapped to atomic-resolution, using geometric projection followed by sets of energy minimization. The protein transmembrane domains were embedded in a biologically relevant lipid bilayer(Zhang et al., 2012) using the CHARMM-GUI (Jo et al., 2008). This composition corresponded to palmitoyloleoyl phosphatidylcholine (POPC), palmitoyloleoyl phosphatidylethanolamine (POPE), and palmitoyloleoyl phosphatidylserine (POPS) in a ratio of ~6:3:1(Zhang et al., 2012). The system was placed in a cubic box of ~25x25x13 nm^3 and solvated with ~180,000 explicit TIP3P[8] water molecules. CHARMM36 parameters were used to treat the lipid(Klauda et al., 2010) and protein(Best et al., 2012). Ca^{2+} cations were added at a 0.1 M concentration, with additional Cl^- ions used to neutralize the overall system charge. The total system size corresponded to ~840,000 atoms. The energy of the system was minimized with 10,000 steps using the steepest descents algorithm with a 0.1 nm step size. Equilibration in the *NVT* ensemble was performed for 5 ns using position restraints on protein heavy atoms with a force constant of 1,000 kJ mol^{-1} nm^{-2}. Multiple sets of subsequent simulations were then performed in the *NPT* ensemble with gradually decreasing force constants on protein heavy atoms, to prevent unrealistic deformation of the pentamer in the absence of the remaining virion assembly: i) 5 ns at 1,000 kJ mol^{-1} nm^{-2}; ii) 5 ns at 800 kJ mol^{-1} nm^{-2}; iii) 5 ns at 600 kJ mol^{-1} nm^{-2}; iv) 5 ns at 400 kJ mol^{-1} nm^{-2}; and v) 180 ns at 200 kJ mol^{-1} nm^{-2}.

All simulations were run using GROMACS 5.1.4 package(Van Der Spoel et al., 2005). Equations of motion were integrated through the Verlet leapfrog algorithm with a 2 fs time step, and bonds connected to hydrogens were constrained with the LINCS algorithm. The cutoff distance was 1.2 nm for the short-range neighbour list and for van der Waal's interactions with a smooth switching function from 0.8 nm. The Particle Mesh Ewald method was applied for long-range electrostatic interactions with a 1.2 nm real space cutoff.[12] The Nose-Hoover thermostat[13,14] and Parinello-Rahman barostat[15] were used to maintain the temperature and pressure at 310 K and 1 bar, respectively. Simulations were performed on an in-house Linux cluster, composed of nodes containing 2 GPUs (Nvidia K20) and 20 CPUs (Intel® Xeon® CPU E5-2680 v2 @ 2.8 GHz) each. Time dependent analyses were performed using GROMACS 5.1.4. Visualization of simulation snapshots used the VMD package.[16] Electrostatic potential calculations were performed using the APBS plugin[17] for the Chimera[18] visualization package. Partial charges were obtained from the AMBER99SB force field. Residues were protonated according to their dominant populations at pH 7.0.

FRET Fluctuation Correlation Spectroscopy Measurements (FRET-FCS)

A 40-base oligonucleotide 5'-GGGTT-$(A)_{30}$-AACCC-3' DNA hairpin-loop was purchased from IDT Technologies (Singapore). Donor fluorophore carboxytetramethylrhodamine (TMR) is attached at its 3' end via a modified cytosine and a six-carbon linker. Acceptor fluorophore indodicarbocyanine (Cy5) is attached at its 5' end via a three-carbon linker. The donor and acceptor form a fluorescence resonance energy transfer pair with a FRET distance (R_0) of ≈5.3 nm. The structure of the fully closed hairpin-loop is illustrated in (Figure S6B).

FRET-FCS experiments were performed on same already mentioned commercial Olympus FV1200 laser scanning confocal microscope (IX83, Olympus, Singapore) using 543 nm continuous wave laser and 488 pulsed lasers for exciting hairpin and doubly labeled viruses, respectively. The beam was focused into the sample by a water immersion objective (× 60, NA 1.2; Olympus, Tokyo, Japan) after being reflected by a dichroic mirror (DM405/485/543/635 band pass, Olympus, Singapore) and the scanning unit. The fluorescence signal for hairpin and doubly labelled viruses were spectrally divided into donor and acceptor channels by a 650DCLP and 560 DCLP dichroic mirrors, respectively. The donor and acceptor fluorescence was recorded, by a set of single molecule avalanche photodiodes (SPADs) (SPCM-AQR-14, PerkinElmer Optoelectronics, Quebec, Canada), through a 615/45 and 670/40 band pass emission filter (Omega, VT), respectively for hairpin. On the other hand, virus's fluorescence was collected through 513/17 and 615/45 band pass emission filter (Omega, VT), respectively. The intensities of the donor and acceptor channel are collated in 20 μs time bins in the SymPhoTime64 software and exported as text files. Using a MATLAB script, the proximity ratio is calculated for each time bin and the autocorrelation of the proximity ratio is calculated. The calculated autocorrelation of the proximity ratio is then fitted using the Levenberg-Marquardt iteration algorithm by Origin 9.1.

QUANTIFICATION AND STATISTICAL ANALYSIS

Where appropriate, statistical details are given in the STAR Methods, Figure legends and Supplemental Information.